

COIN REPORT NUMBER 2023008

ANALYSIS AND OPTIMIZATION OF GAIT CYCLE OF 25-DOF NAO ROBOT USING PARTICLE SWARM OPTIMIZATION AND GENETIC ALGORITHMS

Pushpendra Gupta* and Dilip Kumar Pratihar†

*Mechanical Engineering Department,
Indian Institute of Technology Kharagpur-721302
West Bengal, India*

**pushpendra050@iitkgp.ac.in
†dkpra@mech.iitkgp.ac.in*

Kalyanmoy Deb

*Electrical and Computer Engineering
Michigan State University, East Lansing,
MI 48824, USA
kdeb@egr.msu.edu*

The gait cycle of 25-DOF humanoid robot, namely NAO robot, consists of single support phase (SSP) and double support phase (DSP). Both dynamic and stability analyses are carried out for this robot to determine its power consumption and dynamic stability margin, respectively. Constrained single-objective optimization problems are formulated for the SSP and DSP separately and solved using particle swarm optimization (PSO) and genetic algorithms (GA). A performance index, other than the fitness function, consisting of constraint values and maximum swing height, is also considered to compare PSO and GA-obtained optimal solutions. PSO is able to find the trajectories that offer higher swing height for nearly similar power consumption during SSP. A performance assessment of each algorithm based on the best fitness values in each generation across several runs is also carried out. These values are compared using the Wilcoxon rank-sum test, and PSO is found to be statistically better than GA. The optimal solutions from the simulations are tested using the Webots simulator to validate their efficacy on stability. Moreover, an investigation of the influence of gait parameters on power consumption during SSP and DSP reveals that the humanoid robot with a higher hip height, lower swing height, and slow pace consumes less power. The methodology developed in this is generic and can be easily extended to other robots.

Keywords: NAO Humanoid Robot; Single Support Phase; Double Support Phase; Trajectory Planning; Optimization; Particle Swarm Optimization; Genetic Algorithm

1. Introduction

The humanoid robot mimics humans and walks on two legs for better mobility compared to the wheeled robot and manipulator. It can navigate through a variety of terrains, including stairways, sloping surfaces, obstacles, ditches, etc. These advantages of having better mobility on uneven terrain have attracted many researchers. Research on humanoid robots in bipedal locomotion for efficient and balanced gait planning for optimal power and maximum stability has made substantial progress in the last three decades. NAO, a 25 degree of freedom (DOF) humanoid robot, could attract researchers due to its high walking speed, improved robustness, enhanced endurance, and programming capabilities. Researchers have long been interested in achieving a smooth walking pattern while using less power. Humanoid robot's applications require completing the same task with better stability and less energy. In this study, an attempt is made to determine optimal gait parameters to minimize the power consumption by maintaining the dynamic balance margin (DBM)

of a 25 DOF NAO humanoid robot, version 6, developed by SoftBank robotics. Because a well-balanced gait cycle consuming a high amount of energy is not desirable.

The gait cycle of a biped robot consists of single support phase (SSP) and double support phase (DSP). Most of the available literature on biped robots studied the SSP. Despite being a crucial phase, DSP received less attention, as it consumes about only 20% of the total cycle time. DSP is essential in achieving steady locomotion when walking at a moderate speed compared to high speed.¹ The present work separately studied both cycles, *viz.* SSP and DSP of a 25 DOF NAO humanoid robot. The problem of DSP is solved by considering two separate SSPs.² Most of the studies considered the hip height constant throughout the walking motion; however, in this study, the hip trajectory is planned in x , y , and z directions using cubic polynomial equations. This helps to understand the effect of hip movement in 3D space on an energy-efficient gait cycle. Robots' hip, swing leg, and arm motion were simplified using the cubic polynomial trajectories. SSP or DSP is the phase between two consecutive DSP or SSP, respectively. To link to the next walking phases, position, velocity, and acceleration profiles are required at the start and end of the SSP or DSP. There are very limited studies related to the average speed required to maintain the desired DBM. An average speed is crucial for maintaining a DBM during walking, and at a higher speed, the torque fluctuations are much higher. The motor may fail due to a sudden change in torque within a given period, which may bring some jerky moments to the robot. Only a few studies considered the minimal torque change to produce smoothness in the motion. Hence, a suitable constraint is also considered to address the problem of torque fluctuation during higher speeds. Population-based optimization algorithms depend on the initial population and their respective parameters. However, an optimal solution may vary with the different initial populations. A limited number of studies are available on the arms movement for improving stability. This study also considered the effect of arm swings on dynamic stability. Many investigators have not performed a statistical analysis, which is required to correctly understand their variations and suitability for a problem. The differences in the optimal solution for a problem provided by the algorithm over multiple runs will help in its selection for that problem.

A Constrained single-objective optimization problem is formulated to minimize the power consumption while ensuring the dynamic stability and minimum torque fluctuation. The formulated single-objective optimization problem is solved using Particle Swarm Optimization (PSO) and Genetic Algorithm (GA) to find the optimal gait parameters for minimum power consumption separately during the SSP and DSP. While solving the single-objective optimization problem, the maximum permissible change in torque within a given time interval is considered as a constraint to be satisfied in order to reduce the overloading or failure of the motor. One of the goals of this work is to determine the range of terminal velocities to maintain a desired dynamic balance while using the least amount of power. Minimum sagittal and lateral velocities are found out to keep the robot in motion without falling in SSP and DSP. The movement of both arms has been considered for better dynamic stability. A comparative and statistical analysis have been considered here for both algorithms. Wilcoxon rank-sum test is also performed to find the best algorithm statistically. Finally, a simulation in the Webots simulator has confirmed the stability and reported no violation in the joint limit for the proposed trajectories.

The rest of the paper is organized as follows: Section 2 reviews the existing studies, and the mathematical formulation of the problem is discussed in Section 3. Section 4 deals with the mathematical statement of the single-objective optimization problem. Results are stated and discussed in Section 5, and concluding remarks are presented in section 6.

2. Existing Studies

2.1. Kinematic and Dynamic Analysis

Robot kinematics is basic yet essential to understand the robot's movement in 3D space. Forward Kinematics (FK) deals with mapping the joint space into the 3D space. However, Inverse Kinematics (IK) relates the 3D space to joint space. IK is a relatively more complex task for a high DOF robotic system with its joints placed in series compared to its FK. Many researchers have tried different methodologies to solve the problem of IK. However, an analytical solution is always preferable to an iterative approach due to its accuracy and faster implementation. Researchers solved the IK of the NAO robot using vector algebra³⁻⁵, human mimicking system⁶, the cartesian trajectory of human⁷, and optimization process⁸ to convert the robot configuration from cartesian space to joint space. The inverse kinematics (IK) concept proposed by Nikolaos et al.³ is employed in this study, as it provides exact analytical solutions that are useful for real-time execution.

Dynamic analysis, in addition to kinematic analysis, is essential for improved robot control. Hashemi and Gaffari⁴ focused on kinematic analysis and dynamic modeling by approximating the trajectory using cubic splines for the NAO robot. Joint angles' simulation and inertial forces were verified using experimental results. The inverse dynamics⁵ was carried out in MSC Adams and verified on the NAO robots' lower part with joints' angles as experimental data. Torque

and power calculations are challenging for biped robots due to highly nonlinear dynamics. For the high DOF, several researchers have attempted to solve the dynamics of a humanoid robot using different techniques. Researchers used kinematic human motion data ⁹, SimMechanics of MATLAB toolbox ¹⁰, reference-model-based control design ¹¹, MSC Adams ⁵, PD control law with gravity compensation ¹², Lagrange-Euler formulation ^{13,14}, Newton-Euler equations ¹⁵, Chaotic Recurrent Neural Network ¹⁶, and D'Alembert's-based virtual work principle ¹⁷ to perform the inverse dynamics of biped robot. Lagrange-Euler formulation is used in this study to compute torque demand and average power consumption by the actuators of the NAO robot.

2.2. Stability Analysis

Most bipedal systems had been modeled using analytical balancing techniques to maintain the dynamic balance by taking the help of a basic inverted pendulum (IP) ¹⁸ due to its simplicity, but the concept of the Zero-Moment Point (ZMP) ¹⁹ technique could reach popularity due to its accuracy for the multi-body system. To declare a humanoid is dynamically balanced, the ZMP should always be lying inside the foot support polygon. ZMP computation is crucial at each point to stabilize the walking cycle of a robot. DBM ²⁰, or stability margin, is a positive quantity that indicates how distant the ZMP is from the support polygon. The robot is marginally stable if the ZMP is seen to be extremely close to the support polygon's boundary; nevertheless, a larger value of DBM ensures greater stability.

Chung *et al.* ²¹ improved the existing method of ZMP calculation using Denavit-Hartenberg (DH)-based recursive Lagrangian method. The proposed method accurately evaluated the rate of angular momentum in the ZMP formulation, and a simulation of walking and running motion provided more realistic bipedal motion. Robo-Erectus ²², a humanoid robot, was optimized for ZMP, inertia forces, and geometrical constraints to improve dynamically balanced locomotion, smooth transition, and stable walking. Liu and Urbann ²³ modified the walking pattern of the NAO robot using the three-dimensional motion of the upper body. They experimentally verified that the robot could walk with an almost stretched knee with enhanced dynamic balance.

2.3. Evolutionary Computation-based Studies

Biped locomotion depends on several gait parameters. Researchers explored a range of strategies to reduce the energy consumption of a dynamically balanced gait cycle to determine the best gait parameters. The evaluation of geometric parameters, dynamic calculations, and controllability are highly nonlinear, so evolutionary optimization techniques were utilized to get the optimal parameters. In their review study, Gong *et al.* ²⁴ discussed various potential improvements in the efficiency and quality of evolutionary gait optimization and future research directions. A gait cycle is a synchronized sequence of leg movement consisting of SSP and DSP ²⁵. There are some transition phases between these two phases, viz. contact and swing phase. Figs. 1 (a) through (d) display the walking cycle of a biped robot. In SSP, the robot is supported by a single-leg, whereas in DSP, the robot is supported by both legs. Investigators have put in a lot of effort to explore the influence of SSP and DSP on the dynamically balanced and efficient walking cycle of a two-legged robot.

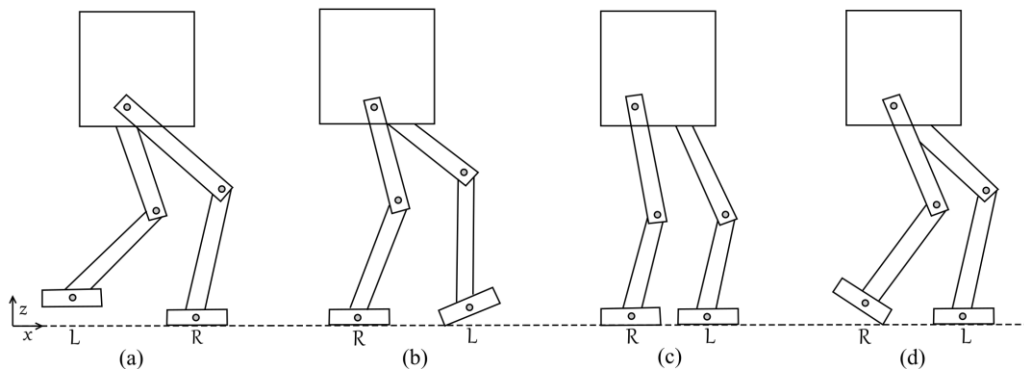


Fig. 1. A schematic view showing four phases of a locomotion cycle of a biped robot: (a) Single Support Phase, (b) Contact Phase, (c) Double Support Phase, (d) Take-Off Phase (where L and R represent left and right feet, respectively)²⁵

Many researchers have studied the effects of SSP on the walking cycle of biped robots. The SSP ²⁶⁻²⁸ was analyzed for ascending and descending staircases using soft-computing approaches to generate dynamically balanced gaits. However, these studies had not considered DSP. Vundavilli and Pratihari ²⁹ had analytically modeled the gait and optimized it to maximize the DBM and minimize the power consumption using neural networks and fuzzy logic-based approaches. They

generated a dynamically balanced gait after considering the SSP and calculating DBM using the ZMP concept for a seven DOF biped robot during ditch crossing. The dynamically balanced gait generation of seven DOF biped robots was solved using genetic-neural and genetic fuzzy systems after analyzing the SSP for sloping surfaces by Vundavilli and Pratihari.³⁰ A few investigators have studied the effects of DSP. Luo and Xia³¹ studied both walking phases (SSP and DSP), and torso motion was controlled to reduce the energy consumption and maximize the dynamic stability at the landing. The simulation confirmed the feasibility of the proposed method. The walking efficiency was better with a forward tilting of the torso, whereas backward tilting increased power consumption. However, the robot movement during DSP was simplified by modeling it as an IP. DSP was analyzed by Rajendra and Pratihari² using PSO and GA during ascending and descending of a staircase. The lateral movement was not considered in this study. Raj et al.³² used Real Coded GA (RCGA) to create an optimal set of walk parameters for the optimization of energy and stability of the NAO robot for SSP, DSP, and transition phases. They demonstrate a trade-off between stability and energy function. However, their investigations for the NAO robot consider a constant hip height from the ground. Many researchers have used PSO and GA to find the optimal trajectories for energy-efficient walking cycles. Dau *et al.*³³ generated optimal hip and foot trajectories using polynomial interpolation. GA was used to find the optimal key parameters to optimize it further to reduce energy consumption. The proposed method was verified on flat and slope walking simulations of NUSBIP-II biped robot. They had not considered the lateral movement. PSO³⁴ was used in the gait optimization for omnidirectional walking on a modified Kondo KHR-1 humanoid robot. They also considered arm movement as well as different walking phases, but no additional optimization approaches were utilized to compare PSO performance. After assuring the least energy consumption, GA³⁵ was used along with the motion/force control scheme to generate the optimal trajectories for the seven-link biped walking on flat ground and sloping terrain. The study found that energy consumption increased with the increase in walking speed. However, a comparison of the performance of GA with different population-based optimization techniques might have been useful in determining better walking parameters.

There had been a few prominent optimization methodologies utilized in decreasing excessive energy consumption, enhancing walking speed, finding the shortest path, and optimizing trajectories. Hemker *et al.*³⁶ and Wolff *et al.*³⁷ had improved the walking speed of a 24 DOF and 17 DOF humanoid robot using the surrogate optimization method and evolutionary procedure, respectively. Muni *et al.*³⁸ used the Bacterial Foraging Optimization Algorithm (BFOA) to build the best navigation for the NAO humanoid robot. BFOA utilizes the foraging ability of bacteria to find the shortest path in the least amount of time. The proposed method was verified using simulation and an experimental platform. The iterative optimization method³⁹ was applied to a seven-link biped robot to solve the high energy consumption. The trunk trajectory was optimized when the given robot followed the desired ZMP trajectory, and then, an energy-efficient gait could be obtained with the security of a balanced cycle. Roussel *et al.*⁴⁰ generated gait patterns, which consumed minimum energy while body mass was concentrated on the hip of the humanoid robot. Silva and Machado *et al.*⁴¹ analyzed energy consumption while keeping hip height and sagittal velocity constant. Channon *et al.*⁴² analyzed the relationship between forward velocity and step length with respect to consumed energy. Uno *et al.*⁴³ took into account not just the least amount of energy utilized but also the minimum change in torque. The former gait resembled human motion more closely, whereas the later gait was more stable due to a smooth shift in link acceleration.

3. Mathematical Formulation of the Problem

Fig. 2 shows the lower and upper parts of the NAO robot with the joint angles' naming convention. It also shows the positions of lumped masses. The lower part of the NAO robot has eleven DOF, whereas the upper part has fourteen DOF. The pelvis joint is made common in both legs. Left and right *HipYawPitch* cannot move independently due to a single actuator moving this joint, which directly affects both the legs. Each leg has two joints at the hip, one joint at the knee, and two joints at the ankle. The *R* and *L* prefixes are used in conjunction with the joint angles' names to indicate their connections to the robot's Right and Left sides, respectively. NAO robot's mass values and dimensions are taken from its official website.^{44,45} r_i represent the Center of Mass (CoM) position vectors⁴⁵ for the concentrated lumped masses m_i in kg on the i^{th} limb.

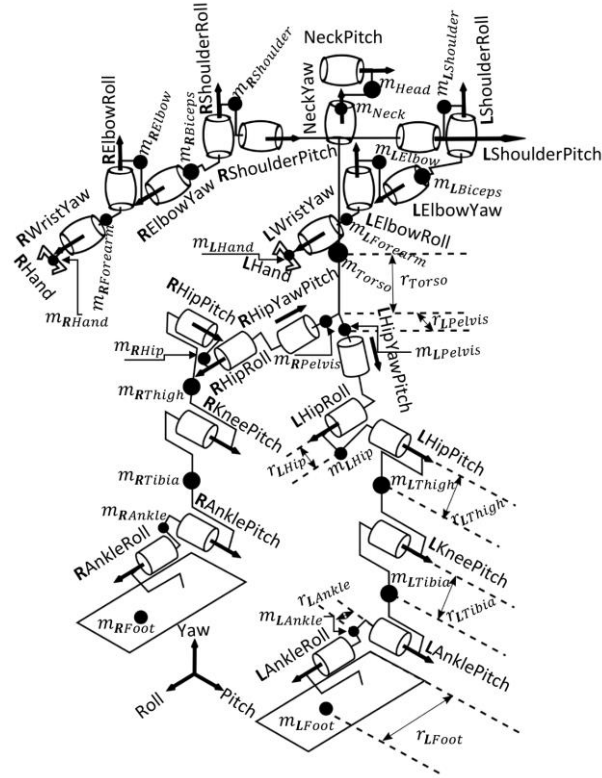


Fig. 2. Line Diagram of the lower and upper parts of the NAO robot with lumped masses, CoM position, and joint angles' naming convention.

The robot's left and right halves are symmetrical, and the masses⁴⁵ of the corresponding limbs are the same on both sides. The NAO robot is made up of 25 lumped masses in total. Each leg consists of six lumped masses *viz.* Pelvis, Hip, Thigh, Tibia, Ankle, and Foot. Shoulder, Biceps, Elbow, Forearm, and Hand are the five lumped masses that make up each arm. Torso, Neck, and Head are the other three-lumped masses. The friction during SSP and DSP is assumed to be sufficient to prevent slipping.

3.1. Single support phase

Fig. 3 shows the kinematic model for the lower and upper parts of the NAO robot during SSP. The swing leg trajectory is shown to move from x_i to x_f and attended a maximum swing height (S_h^{max}) in the mid of the trajectory. Z_H is the hip height. DH parameters are used to assign a coordinate system to each joint of the robot, and kinematic analysis is carried out to realize the humanoid robot's motion. Four parameters²⁵ of classic DH convention, namely θ_i , d_i , a_i and α_i are used in translating the coordinate from $(i-1)^{th}$ link to i^{th} link. The transformation matrix of the i^{th} link with respect to $(i-1)^{th}$ link is expressed as follows:

$$T_{i-1}^i = Rot(z, \theta_i) Trans(z, d_i) Rot(x, \alpha_i) Trans(x, a_i) \quad (1)$$

Fig. 4 shows the overall dimensions of a 25 DOF Humanoid Robot, consisting of two legs, two hands, one torso, and one neck. It also shows DH parameter settings for the lower and upper parts of the robot. Tables 1 and 2 contain the information related to the link and joint parameters for the left and right leg, respectively. All the dimensions are in *mm*. The hip joint is located in the *y*-direction from the Pelvis at 50 *mm* (left hip) and -50 *mm* (right hip). The *z*-offset from the Pelvis is kept equal to 85 *mm*. Length l_1 and l_2 represent thigh and tibia lengths, respectively. The IK solution for the left leg chain is explained below. The left leg chain is considered as a serial manipulator, where the left leg foot serves as the origin/base frame, and the torso is treated as an end-effector. The concept of carrying out the IK for NAO is taken from Kofinas *et al.*³. $A(P_x, P_y, P_z)$ denotes the translation in *x*, *y*, and *z* directions by P_x , P_y , and P_z , respectively. $R_k(\phi)$ represents the rotation matrix about k^{th} axis by an angle ϕ .

Table 1. DH Parameters for left leg chain from *LFoot* to Pelvis

Joint	Frame	θ	d	α	a
Base	<i>LFoot</i>		$A(0, 0, 45.19)$		
	Rotation matrix		$R_y(\pi/2) R_z(-\pi)$		
1	<i>LAnkleRoll</i>	θ_6	0	$\pi/2$	0
2	<i>LAnklePitch</i>	θ_5	0	0	$l_2(102.90)$
3	<i>LKneePitch</i>	θ_4	0	0	$l_1(100)$
4	<i>LHipPitch</i>	θ_3	0	$-\pi/2$	0
5	<i>LHipRoll</i>	$\theta_2 - \pi/4$	0	$\pi/2$	0
6	<i>LHipYawPitch</i>	$\theta_1 + \pi/2$	0	$3\pi/4$	0
	Pelvis		$A(0, -50, 85)$		

Table 2. DH Parameters for right leg chain from Pelvis to *RFoot*

Joint	Frame	θ	d	α	a
Base	<i>Pelvis</i>		$A(0, -50, -85)$		
	Rotation matrix		$R_x(-\pi/4)$		
1	<i>RHipYawPitch</i>	$\theta_1 - \pi/2$	0	$-\pi/2$	0
2	<i>RHipRoll</i>	$\theta_7 - \pi/4$	0	$\pi/2$	$-l_1(100)$
3	<i>RHipPitch</i>	θ_8	0	0	$-l_2(102.90)$
4	<i>RKneePitch</i>	θ_9	0	0	0
5	<i>RAnklePitch</i>	θ_{10}	0	$-\pi/2$	0
6	<i>RAnkleRoll</i>	θ_{11}	0	0	0
	Rotation matrix		$R_z(\pi) R_y(-\pi/2)$		
	<i>RFoot</i>		$A(0, 0, -45.19)$		

Let T_i^j denotes the transformation matrix of j^{th} joint with respect to i^{th} joint. then T_{LFoot}^{Pelvis} is given by

$$T = A_{LFoot}^0 R_y\left(\frac{\pi}{2}\right) R_z(-\pi) T_0^1 T_1^2 T_2^3 T_3^4 T_4^5 T_5^6 A_6^{Pelvis} \quad (2)$$

After removing the known homogeneous transformation matrices A_{LFoot}^0 and A_6^{Pelvis} by pre- and post-multiplication to T maintaining their sequence. The new transformation matrix is denoted by \hat{T} . A post-multiplication to \hat{T} by $-\pi/4$ in the x -axis will help in aligning the z -axis with the yaw joint, and that transformation matrix is denoted by \tilde{T} . Both homogenous transformation matrices (\hat{T} and \tilde{T}) are given below.

$$\hat{T} = (A_{LFoot}^0)^{-1} T (A_6^{Pelvis})^{-1} \quad (3)$$

$$\tilde{T} = \hat{T} R_x\left(-\frac{\pi}{4}\right) \quad (4)$$

If the hip position is set at the origin, then d denotes the distance between the hip and ankle joint as

$$d = \sqrt{\left[(0 - \tilde{T}_{(1,4)})^2 + (0 - \tilde{T}_{(2,4)})^2 + (0 - \tilde{T}_{(3,4)})^2\right]} \quad (5)$$

The IK of the NAO Robot is solved analytically³ using vector algebra to convert the robot configuration from Cartesian space to joint space as given below.

$$\theta_4 = \pm \left(\pi - \cos^{-1} \left(\frac{l_1^2 + l_2^2 - d^2}{2l_1 l_2} \right) \right) \quad (6)$$

$$\theta_6 = \tan^{-1} \left(-\frac{\tilde{T}_{(2,4)}}{\tilde{T}_{(3,4)}} \right) \quad (7)$$

$$T' = \left(R_y\left(-\frac{\pi}{2}\right) R_z(-\pi) \right)^{-1} \tilde{T} \quad (8)$$

$$\theta_5 = \sin^{-1} \left(\frac{T'_{(2,4)}(l_2 + l_1 \cos \theta_4) - l_1 T'_{(1,4)} \sin \theta_4}{l_1^2 \sin^2 \theta_4 + (l_2 + l_1 \cos \theta_4)^2} \right) \quad (9)$$

$$\theta_5 = \pi - \sin^{-1} \left(\frac{T'_{(2,4)}(l_2 + l_1 \cos \theta_4) - l_1 T'_{(1,4)} \sin \theta_4}{l_1^2 \sin^2 \theta_4 + (l_2 + l_1 \cos \theta_4)^2} \right) \quad (10)$$

$$T'' = (T_1^2 T_2^3)^{-1} T' \quad (11)$$

$$\theta_2 = \frac{\pi}{4} - \cos^{-1} T''_{(3,2)} \quad (12)$$

$$\theta_1 = \sin^{-1} \left(-\frac{T''_{(3,3)}}{\sin \left(\theta_2 - \frac{\pi}{4} \right)} \right) - \frac{\pi}{2} \quad (13)$$

$$\theta_3 = \cos^{-1} \left(\frac{T''_{(1,2)}}{\sin \left(\theta_2 - \frac{\pi}{4} \right)} \right) \quad (14)$$

Eqs. (6) to (14) are used to find the joint angles for the left leg. Similarly, the required joint angles are computed using IK analytical solution³ to reach *RFoot* from the known *Pelvis*.

When the robot is walking and considering only one walking cycle for the movement on plain ground, the joint angle is calculated from the hip and swing leg trajectories using IK. The joint angles from IK are utilized to carry out inverse dynamics. To compute torque requirements at different motors of the NAO robot, various components, such as inertia, Coriolis/centrifugal, and gravity, are taken into account. The angular velocity and acceleration of the joints are determined by numerical differentiation as per the given time interval.

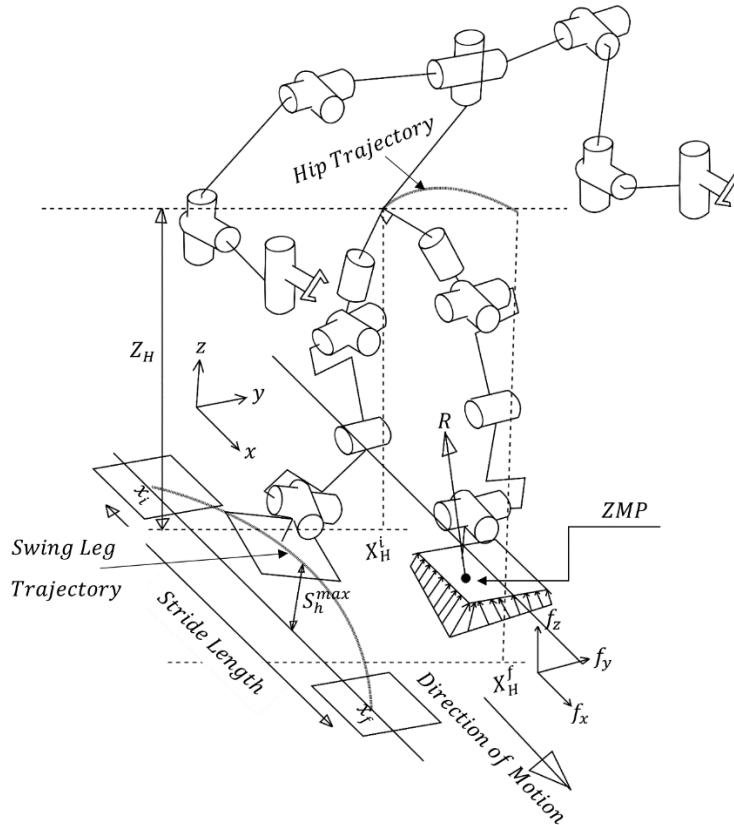


Fig. 3. A schematic view of the upper and lower part of the NAO robot during the Single Support Phase.

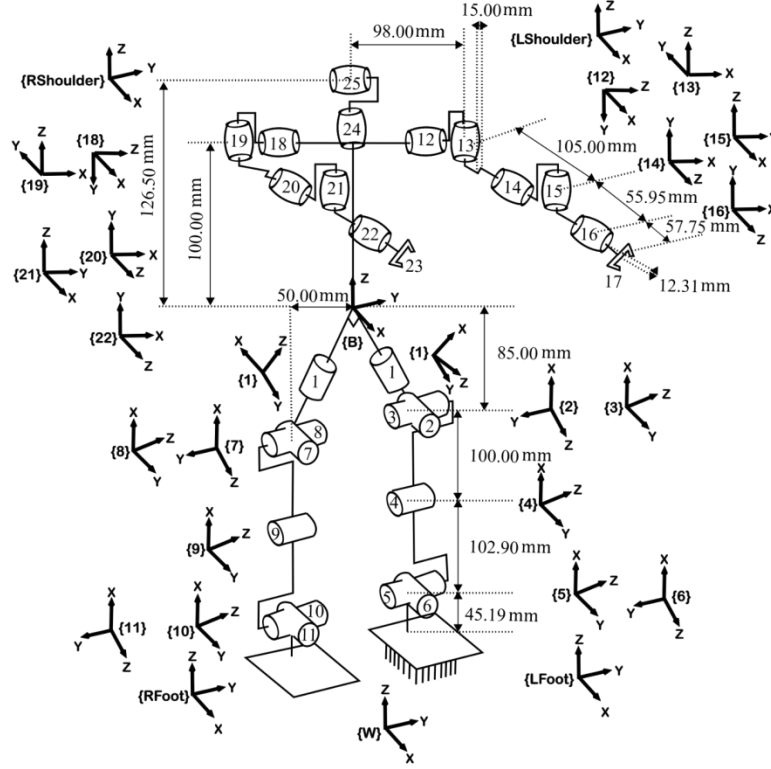


Fig. 4. DH Parameter setting and overall dimensions for the upper and lower part of the NAO robot.

The inverse dynamics is solved using the Lagrange-Euler formulation⁴⁶ as given in Eq. (15).

$$\tau_i = \sum_{c=1}^n D_{ic} \ddot{q}_c + \sum_{c=1}^n \sum_{d=1}^n h_{icd} \dot{q}_c \dot{q}_d + C_i \quad (15)$$

where $i = 1, 2, \dots, n$ joints. D_{ic} , h_{icd} , and C_i represent inertia, coriolis and centrifugal, and gravity terms, respectively, whose expressions are given in Eqs. (16) to (18).

$$D_{ic} = \sum_{j=\max(i,c)}^n \text{Tr}(U_{jc} J_j U_{ji}^T) \quad (16)$$

$$h_{icd} = \sum_{j=\max(i,c,d)}^n \text{Tr}(U_{jcd} J_j U_{ji}^T) \quad (17)$$

$$C_i = \sum_{j=i}^n (-m_j \bar{g} U_{ji}^T \bar{r}_j) \quad (18)$$

where $i, c, d = 1, 2, \dots, n$ joints. J is the inertia tensor; $U_{ij} = \partial^0 T / \partial q_j$; \bar{g} is the gravity column matrix, which is along the negative z -direction; m_i is the mass of i^{th} link. \bar{r}_j is the CoM position vector for the j^{th} link. The whole robot is considered a seven-link model for dynamic analysis consisting of the left foot, left lower leg, left upper leg, torso, right upper leg, right lower leg, and right foot. It is assumed for the purpose of analysis to be a serial manipulator of 12 DOF starting from left foot (*LFoot*) to right foot (*RFoot*) (although eleven independent motors are connected to these joints and the pelvis joint is made common to both the legs). *LFoot* is taken as a base, and the torso is considered as the end-effector of a serial manipulator, and after reaching the torso, the *RFoot* is considered as end-effector. Because the robot is walking in a straight path, both legs' hip yaw pitch angles are almost zero. Torque variations for both arms are also computed using Eq. (15). The force distributions of the foot on the ground could be reduced to the resultant force R , the point of attack, which needs to be in the sole of support polygon, as shown in Figs. 3 and 5.

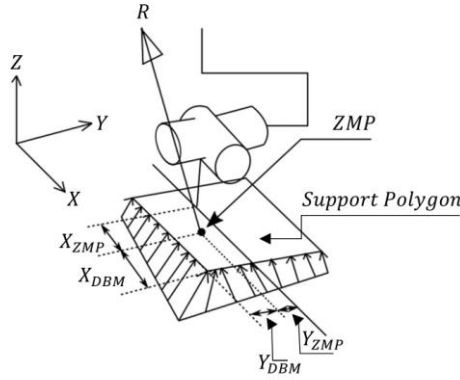


Fig. 5. Definition of Zero Moment Point and Dynamic Balance Margin ⁴⁷

The ZMP is a location on the ground where the sum of all moments of forces and momentums becomes equal to zero. ZMP lying within the supporting polygon's sole helps the biped to keep it in its stable position. X_{ZMP} and Y_{ZMP} represent ZMP in x (along the length of the foot) and y (along the width of the foot) directions, respectively. ZMP along the x and y -axes can be determined using Eqs. (19) and (20). I_i denotes the moment of inertia of i^{th} joint (in $\text{kg}\cdot\text{m}^2$), $\dot{\omega}_i$ is the angular acceleration of joint i (in rad/s^2), m_i denotes the mass of i^{th} joint (in kg), (x_i, z_i) are the coordinates of i^{th} lumped mass, g is the acceleration due to gravity (in m/s^2), n is the total number of joints, \ddot{z}_i is the acceleration of i^{th} lumped mass in the z -direction (m/s^2), and \ddot{x}_i is the acceleration of i^{th} lumped mass in the x -direction (m/s^2) ⁴⁸.

The forward and sideways motion of the robot are considered in x and y -direction, respectively. z -axis is taken along the height of the robot. As previously stated, DBM is the minimum distance between the ZMP points and the support polygon's boundary, and X_{DBM} and Y_{DBM} represent the DBM in x and y direction, respectively. DBM in x and y directions are calculated using Eqs. (21) and (22) based on support leg position and ZMP points. Moreover, the combined CoM of the whole robot is calculated using Eq. (23). DH parameters are useful in finding the CoM position of each link. In Eq. (23), $p_i \in \mathbb{R}^{3 \times 1}$ is the position of the center of i^{th} mass. $m_i \dot{p}_i$ is the momentum of the i^{th} point mass. Differentiating the Eq. (23) yields Eq. (24). Total momentum P' of the robot by considering all the point masses is given in Eq. (25). The relationship between the velocity of the robot and linear momentum can be easily established using Eqs. (24) and (25). The equation of the translation motion of the robot can be obtained by differentiating Eq. (25) with respect to time. $m_i \ddot{p}_i$ is the external force (f_i) in N acting on the i^{th} point mass. The sum of all the external forces acting on the robot is denoted by F in Eq. (26). The gravitational force is equally applied to all the lumped masses of the body and will always be there regardless of the robot's motion; hence it can be considered separately from all other forces. The acceleration due to gravity is taken in the negative z -direction, and it is set equal to $[0, 0, -9.8]^T$ in Eq. (27). M is the total mass of the robot in kg . $f \in \mathbb{R}^{3 \times 1}$ represent the ground reaction force (represented by R in Figs. 3 and 5) and has its component in x, y , and z -direction. Fig. 6 shows the foot dimensions, lower and upper bounds of ZMP values based on the foot coordinates.

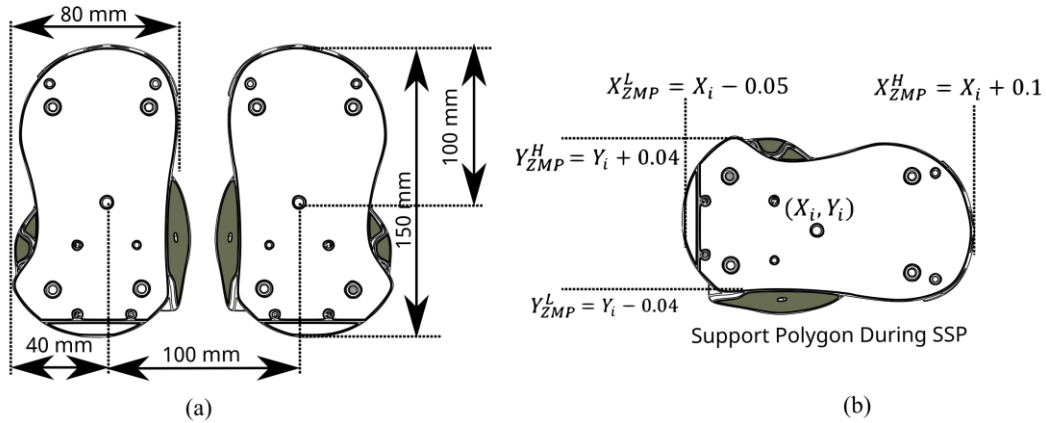


Fig. 6. (a) NAO Robot foot dimension and (b) ZMP's higher and lower bound based on the support leg coordinate. Superscript H and L represent the highest and lowest ZMP possible in the x and y directions based on the foot coordinates. The darker region shows a safe zone.

$$X_{ZMP} = \frac{\sum_{i=1}^{i=n} I_i \ddot{\omega}_i + m_i x_i (\ddot{z}_i - g) - m_i \ddot{x}_i z_i}{\sum_{i=1}^{i=n} m_i (\ddot{z}_i - g)} \quad (19)$$

$$Y_{ZMP} = \frac{\sum_{i=1}^{i=n} I_i \ddot{\omega}_i + m_i y_i (\ddot{z}_i - g) - m_i \ddot{y}_i z_i}{\sum_{i=1}^{i=n} m_i (\ddot{z}_i - g)} \quad (20)$$

$$X_{DBM} = \begin{cases} (X_i + 0.1) - X_{ZMP}, & \text{if } X_{ZMP} \in [X_i, X_i + 0.1] \\ X_{ZMP} - (X_i - 0.05), & \text{if } X_{ZMP} \in [X_i - 0.05, X_i] \\ 0 & \text{otherwise} \end{cases} \quad (21)$$

$$Y_{DBM} = \begin{cases} (Y_i + 0.04) - Y_{ZMP}, & \text{if } Y_{ZMP} \in [Y_i, Y_i + 0.04] \\ Y_{ZMP} - (Y_i - 0.04), & \text{if } Y_{ZMP} \in [Y_i - 0.04, Y_i] \\ 0 & \text{otherwise} \end{cases} \quad (22)$$

$$C = \frac{\sum_{i=1}^n m_i p_i}{\sum_{i=1}^n m_i} \quad (23)$$

$$\dot{C} = \frac{\sum_{i=1}^n m_i \dot{p}_i}{\sum_{i=1}^n m_i} \quad (24)$$

$$P' = \sum_{i=1}^n m_i \dot{p}_i \quad (25)$$

$$\dot{P}' = \sum_{i=1}^n m_i \ddot{p}_i = \sum_{i=1}^n f_i$$

$$\dot{P}' = F \quad (26)$$

$$\dot{P}' = Mg + f \quad (27)$$

ZMP is important to verify that the generated gait is dynamically stable. Moreover, the locomotion of a biped robot to move from one place to another place requires suitable trajectory planning for the swing leg and hip to move ahead. Gait Pattern generation directly influences the quality of motion for a biped robot. As shown in Fig. 3, the swing leg's trajectory is designed using the cubic polynomial. These trajectories defined the forward advancement at any given point. The initial and final velocities are taken as zero to avoid any jerky movement. The swing leg's ankle trajectory for right leg can be represented by $[X_A(t), -0.05, Z_A(X_A)]^T$. $X_A(t)$ is the x -coordinate of the ankle position in the sagittal plane as a function of time and $Z_A(X_A)$ is the movement of z -coordinates based on x -coordinates; it helped in moving the leg in a vertical direction according to its x -coordinates. Here, both x and z -coordinates are assumed to follow cubic polynomials. Similarly, hip trajectory in 3D space can be represented by $[X_H(t), Y_H(t), Z_H(t)]^T$. Hip motion in the sagittal, lateral, and vertical directions is planned as a cubic polynomial. Since the right leg is the swing leg during SSP, the right arm is moved in the opposite direction of the robot's movement. Only *ShoulderPitch* and *ElbowRoll* are utilized during the motion. *ShoulderRoll* is kept constant at -0.26 rad for the right and 0.26 rad for the left arm. *RElbowYaw* is kept fixed at 1.5 rad for the right and -1.5 rad for the left arm. Left and right Wrist Yaw are kept at zero. Shoulder pitch and Elbow

Roll movement are assumed to follow cubic polynomials. Four boundary conditions are required for ankle, hip, and arm trajectories to find all the coefficients.

Table 3 lists all the cubic trajectories and their respective boundary conditions for ankle, hip, and arm motion to find the unknown coefficients. Here, t_i denotes the initial time. t_f is the final time duration for one cycle. x_i and x_f are the initial and final positions of the swing leg, respectively. where $x_f = x_i + S_L$; and S_L is the Step Length kept equal to 0.06 m. These two values, namely x_i and x_f are dependent on the distance covered by the swing leg. The swing leg traveled a distance from x_i to x_f equal to Stride length. S_h^{max} denotes the maximum swing height achieved at the mid of the swing leg trajectory. The support leg is kept fixed at $\left[x_i + \frac{x_f}{2}, 0.05, 0\right]^T$ during the entire swing leg movement. The hip traveled from $X_H(t_i)$ to $X_H(t_f)$. h represents the initial and final hip height and is kept as same for the repeatability condition. V_s^X, V_s^Y and V_s^Z are the starting velocities in x, y , and z -directions, respectively. V_e^X, V_e^Y and V_e^Z are the end velocities in x, y , and z -directions, respectively. After getting the hip and swing leg trajectories, IK is used to find the joint angles of both the legs to reach the desired hip and swing foot position. Arm movements are provided directly at the joint space. The DH Parameter setting for the left and right arms is shown in Fig. 4. The joint and link parameters (in mm) for the left arm are given in Table 4. Shoulder offset Y (98 mm) and Elbow Offset Y (15 mm) need to be taken negative for the right arm.

Table 3. Swing leg, ankle, hip, and arms trajectory planning, and their respective boundary conditions

Sr. No.	Ankle, hip, and arm's trajectories	Boundary conditions
1 ^c	$X_A(t) = a_0 + a_1 t + a_2 t^2 + a_3 t^3$	$X_A(t_i) = x_i, X_A(t_f) = x_f, \dot{X}_A(t_i) = 0, \dot{X}_A(t_f) = 0$
2 ^c	$Z_A(t) = b_0 + b_1 X_A + b_2 X_A^2 + b_3 X_A^3$	$Z_A(x_i) = 0, Z_A(x_i + S_L) = 0, Z_A(x_m) = S_h^{max}, \dot{Z}_A(x_m) = 0$
3 ^c	$X_H(t) = x_0 + x_1 t + x_2 t^2 + x_3 t^3$	$X_H(t_i) = x_i + x_f/4, X_H(t_f) = x_i + 3x_f/4, \dot{X}_H(t_i) = V_s^X, \dot{X}_H(t_f) = V_e^X$
4 ^c	$Y_H(t) = y_0 + y_1 t + y_2 t^2 + y_3 t^3$	$Y_H(t_i) = 0.025 \text{ m}, Y_H(t_f) = 0.025 \text{ m}, \dot{Y}_H(t_i) = V_s^Y, \dot{Y}_H(t_f) = V_e^Y$
5 ^c	$Z_H(t) = z_0 + z_1 t + z_2 t^2 + z_3 t^3$	$Z_H(t_i) = h, Z_H(t_f) = h, \dot{Z}_H(t_i) = V_s^Z, \dot{Z}_H(t_f) = V_e^Z$
6 ^j	$\theta_{12}(t) = q_0 + q_1 t + q_2 t^2 + q_3 t^3$	$\theta_{12}(t_i) = 2 \text{ rad}, \theta_{12}(t_f) = 1 \text{ rad}, \dot{\theta}_{12}(t_i) = 0, \dot{\theta}_{12}(t_f) = 0$
7 ^j	$\theta_{15}(t) = \alpha_0 + \alpha_1 t + \alpha_2 t^2 + \alpha_3 t^3$	$\theta_{15}(t_i) = -0.42 \text{ rad}, \theta_{15}(t_f) = -0.64 \text{ rad}, \dot{\theta}_{15}(t_i) = 0, \dot{\theta}_{15}(t_f) = 0$
8 ^j	$\theta_{18}(t) = \beta_0 + \beta_1 t + \beta_2 t^2 + \beta_3 t^3$	$\theta_{18}(t_i) = 1 \text{ rad}, \theta_{18}(t_f) = 2 \text{ rad}, \dot{\theta}_{18}(t_i) = 0, \dot{\theta}_{18}(t_f) = 0$
9 ^j	$\theta_{21}(t) = \gamma_0 + \gamma_1 t + \gamma_2 t^2 + \gamma_3 t^3$	$\theta_{21}(t_i) = 0.64 \text{ rad}, \theta_{21}(t_f) = 0.42 \text{ rad}, \dot{\theta}_{21}(t_i) = 0, \dot{\theta}_{21}(t_f) = 0$

^cTrajectories are planned in cartesian space, ^jtrajectories are planned in joint-space

Table 4. DH Parameters for the left-arm chain from *LShoulder* to *LHand*

Joint	Frame	θ	d	α	a
Base	<i>LShoulder</i>		$A(0, 98, 100)$		
	Rotation matrix		$R_x(-\pi/2)$		
1	<i>LShoulderPitch</i>	θ_{12}	0	$\pi/2$	0
2	<i>LShoulderRoll</i>	$\theta_{13} + \pi/2$	0	$\pi/2$	15
	Translation in z-axis		$A(0, 0, 105)$		
3	<i>LElbowYaw</i>	θ_{14}	0	$-\pi/2$	0
4	<i>LElbowRoll</i>	$\theta_{15} - \pi/2$	-12.3	0	55.95
	Rotation matrix		$R_z(\pi/2) R_y(\pi/2)$		
5	<i>LWristYaw</i>	θ_{16}	57.75	$-\pi/2$	0
	<i>LHand</i>	$-\pi/2$	0	0	0

All the starting and end velocities in x, y , and z directions are taken as decision variables, along with the hip height. Also, maximum swing height and time spent in SSP are considered as decision variables for stable gait planning.

3.2. Double support phase

The DSP is analyzed using the concept of Rajendra and Pratihari². The schematic view of DSP is shown in Fig. 7. All the length, mass, and CoM position vectors are kept the same as that, as discussed above for the SSP. The DSP is assumed to be consisting of two SSPs, for the purpose of analysis. X_L and X_R denote the distance of the projected point of the trunk mass from the left and right foot, respectively, in the sagittal plane. Similarly, Y_L and Y_R represent the distance of the projected point of the trunk mass from the left and right foot, respectively, in the lateral plane. The robot with 23 lumped masses (six on each leg, five on each arm and torso) is modeled as two serial manipulators having 12 masses each. On the torso, the neck and head masses are also taken into account. The movement of the robot and its dynamic balance are considered in both directions. The first SSP considered the left leg, left arm, and torso. At the same time, the second SSP is considered by taking the right leg, right arm, and torso. In DSP, the robot carries its total weight on both legs. The torso

mass m_{Torso} is distributed in two parts, namely m_{TorsoL} and m_{TorsoR} on the left and right legs, respectively. The load of the robot is distributed in the lateral plane based on the position of foot placement as given in Eqs. (28) and (29).

$$m_{TorsoL} = \frac{m_{Torso} Y_L}{Y_L + Y_R} \quad (28)$$

$$m_{TorsoR} = \frac{m_{Torso} Y_R}{Y_L + Y_R} \quad (29)$$

Similarly, it can be distributed in a sagittal plane based on foot position. f_L and f_R are the ground reaction force vectors acting between the tip of the leg and the ground, passing through the ZMP. The forces f_L and f_R are acting on the left and right leg, respectively. The feet are assumed to have hard point contacts with friction with the ground. f_{Lx} , f_{Ly} and f_{Lz} are the components of ground reaction force f_L in x , y , and z -direction, respectively, whereas f_{Rx} , f_{Ry} and f_{Rz} are the components of ground reaction force f_R in x , y , and z -direction, respectively. The external force vector F acting on the robot is assumed to have the components as $F = [F_x, F_y, F_z]^T$, which can be calculated using Eq. (26). The earlier study² used a composition method⁴⁹ to determine the biped robot's stability. They determined the whole model's ZMP by considering the intersection point of these two forces. If the forces were found to be parallel, then a concept of Virtual ZMP⁵⁰ was also introduced on non-coincidental planes.

This study utilized a slightly different approach. Forces and moments are balanced using a similar approach utilized for the SSP to find the ground reaction force and ZMP points separately for the left and right foot. Two ZMP positions are initially determined using Eqs. (19) and (20) for the left and right legs after considering it as two SSPs. The value of n in Eqs. (19) and (20) is taken as 12, m_{Torso} is replaced by m_{TorsoL} or m_{TorsoR} , depending on the left or right leg analysis, respectively. The determined p_L and p_R are the ZMP positions of left and right leg, respectively as shown in Fig. 7. Since the robot is assumed to walk on a flat surface, both p_{Lz} and p_{Rz} are kept equal to zero. The whole model's ZMP is determined by setting the x and y components of the moment about point $p = [p_x, p_y, p_z]^T$ to zero⁵¹. The equation is solved (Eqs. (30) and (31)) for p_x and p_y as follows:

$$p_x = \frac{p_{Lx} f_{Lz} + p_{Rx} f_{Rz}}{f_{Lz} + f_{Rz}} \quad (30)$$

$$p_y = \frac{p_{Ly} f_{Lz} + p_{Ry} f_{Rz}}{f_{Lz} + f_{Rz}} \quad (31)$$

where

$$p_L = [p_{Lx}, p_{Ly}, p_{Lz}]^T$$

$$p_R = [p_{Rx}, p_{Ry}, p_{Rz}]^T$$

p is the position of the combined ZMP during DSP, and the value of p_z is taken as zero in Eqs. (30) and (31). If the right leg becomes the swing leg, the vertical component of ground reaction force (f_{Rz}) will be equal to zero, then p_x and p_y in Eqs. (30) and (31) would coincide with the ZMP of the left leg (Support Leg) and be considered as p_{Lx} and p_{Ly} , respectively. It is to be noted that if the hip position lies within the double support polygon, then the robot will be dynamically balanced. However, to be stable during static standing, CoM's vertical projection on the ground should coincide with the ZMP lying within the support polygon⁵¹. DBM during DSP is determined, as shown in Fig. 8 (b).

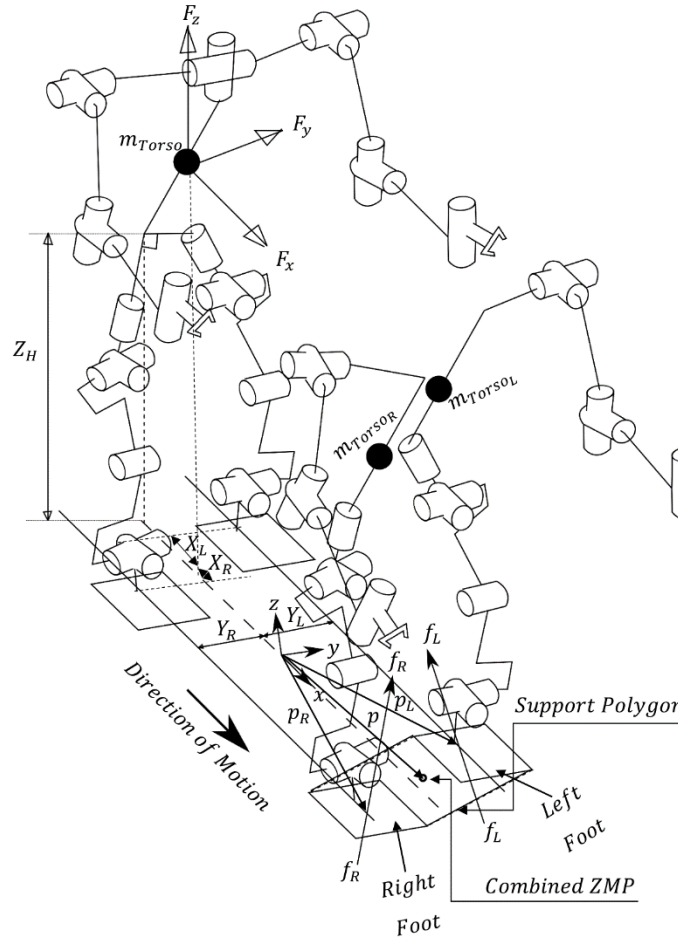


Fig. 7. A schematic view during the Double Support Phase

The hip trajectory in the DSP followed a similar cubic polynomial, as explained during SSP. Once the hip trajectory and location of both feet are known, IK is utilized to find the joint angles required to reach the hip location from its foot position. Eqs. (6) to (14) could be used to find the joint angles for the left leg and a similar methodology can be utilized for the right leg except the α_6 , which would be equal to $3\pi/4$, and *HipoffsetY* (50 mm) and *HipoffsetZ* (85 mm) should be positive. The position of the hip is found with respect to ankle joints. The hip trajectory is assumed to follow cubic polynomial, as given in Table 5. The hip is moved from the position $[0.07, 0.025, Z_H]^T$ to $[0.11, -0.025, Z_H]^T$. The arms' movements are also provided, similar to SSP. Shoulder Roll, Elbow Yaw, Wrist Yaw are kept constant, as discussed above in SSP. Shoulder pitch and Elbow Roll movement are considered as cubic polynomials in the joint space, and to find the unknown coefficients, their respective boundary conditions are listed in Table 5.

Table 5. Hip and arm's trajectory planning and their respective boundary conditions to find unknown coefficients.

Sr. No.	Hip, and arm's Trajectories	Boundary conditions
1 ^c	$X_H(t) = x_0 + x_1 t + x_2 t^2 + x_3 t^3$	$X_H(t_i) = 0.07 \text{ m}, X_H(t_f) = 0.11 \text{ m}, \dot{X}_H(t_i) = V_s^x, \dot{X}_H(t_f) = V_e^x$
2 ^c	$Y_H(t) = y_0 + y_1 t + y_2 t^2 + y_3 t^3$	$Y_H(t_i) = 0.025 \text{ m}, Y_H(t_f) = -0.025 \text{ m}, \dot{Y}_H(t_i) = V_s^y, \dot{Y}_H(t_f) = V_e^y$
3 ^c	$Z_H(t) = z_0 + z_1 t + z_2 t^2 + z_3 t^3$	$Z_H(t_i) = h, Z_H(t_f) = h, \dot{Z}_H(t_i) = V_s^z, \dot{Z}_H(t_f) = V_e^z$
4 ^j	$\theta_{12}(t) = q_0 + q_1 t + q_2 t^2 + q_3 t^3$	$\theta_{12}(t_i) = 1 \text{ rad}, \theta_{12}(t_f) = 1.5 \text{ rad}, \dot{\theta}_{12}(t_i) = 0, \dot{\theta}_{12}(t_f) = 0$
5 ^j	$\theta_{15}(t) = \alpha_0 + \alpha_1 t + \alpha_2 t^2 + \alpha_3 t^3$	$\theta_{15}(t_i) = -0.64 \text{ rad}, \theta_{15}(t_f) = -0.50 \text{ rad}, \dot{\theta}_{15}(t_i) = 0, \dot{\theta}_{15}(t_f) = 0$
6 ^j	$\theta_{18}(t) = \beta_0 + \beta_1 t + \beta_2 t^2 + \beta_3 t^3$	$\theta_{18}(t_i) = 2 \text{ rad}, \theta_{18}(t_f) = 1.5 \text{ rad}, \dot{\theta}_{18}(t_i) = 0, \dot{\theta}_{18}(t_f) = 0$
7 ^j	$\theta_{21}(t) = \gamma_0 + \gamma_1 t + \gamma_2 t^2 + \gamma_3 t^3$	$\theta_{21}(t_i) = 0.42 \text{ rad}, \theta_{21}(t_f) = 0.50 \text{ rad}, \dot{\theta}_{21}(t_i) = 0, \dot{\theta}_{21}(t_f) = 0$

^cTrajectories are planned in cartesian space, ^jtrajectories are planned in joint-space

In DSP, the torso mass is divided into two parts, as explained above. When the hip is positioned between the legs, the mass values change based on its distance from the right and left foot. The lesser the distance from its next support leg, the more will be the torso mass for that leg. Just before this stage, the right leg was the swing leg, and in DSP, it touched the

ground, and the torso started to shift from the left to the right leg. The torso mass is distributed on both legs using Eqs. (28) and (29). The left and right legs are considered as serial manipulators of 6 DOF each. Joint angles are calculated using IK as explained above, for the left and right legs. The obtained joint angles are used to compute torque requirements using Eq. (15) separately for the left and right legs. Similarly, torque variations for both arms are also computed using Eq. (15). The DBM can be calculated after getting the combined ZMP points. The support polygon during DSP is larger than SSP, as shown in Fig 8.

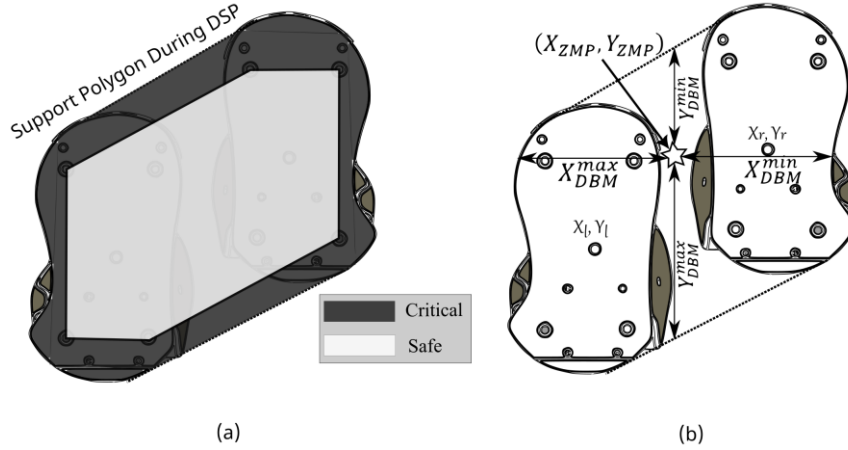


Fig. 8. *a)* Support polygon during Double Support Phase with Critical and Safe Zone for the ZMP points. *b)* minimum X_{DBM} and Y_{DBM} values based on left foot, right foot, and ZMP coordinates. $[X_l, Y_l]$ and $[X_r, Y_r]$ are the left and right foot coordinates.

Thus, the stability margin is higher in DSP, and the robot can take a higher speed to shift the torso from one leg to another. The area shown in the lighter and darker color marked the safe and critical regions for ZMP points, respectively, as shown in Fig. 8(a). The DBM is calculated during DSP by considering the minimum stability margin available in x and y -direction. The minimum distance considered for DBM during DSP will determine whether the robot will be stable or not. It is decided based on the ZMP points, left foot, and right foot coordinates, as shown in Fig. 8(b).

4. Mathematical Statement of Single Objective Optimization

A single-objective optimization problem is formulated to reduce power consumption by maintaining dynamic stability and not exceeding a predefined maximum torque fluctuation during SSP and DSP separately. Moreover, each of the joint angles should lie within its respective range.

4.1. Single support phase

When the robot is studied in the SSP, the predefined values for the initial (X_H^i) and final (X_H^f) hip locations are provided in x -direction. The y -coordinate is kept fixed for both initial and final hip locations. The lateral sway motion of the hip is also considered to realize a 3D dynamic walking of the robot. Here, the robot is changing direction along the y -axis (refer to Fig. 3), and a positive and negative velocities will help to change the direction. However, the velocity (in the sagittal plane) must be positive throughout the walking motion when moving in a forward direction. For velocity in the x -direction, we can take only positive values. Similar to vertical motion, if the hip height needs to be traveled upward or downward, a different combination of velocity is required. For carrying out the analysis in SSP, the Left foot having the coordinates of $[0.06, 0.05, 0]^T$ is considered as a support leg. The Right leg (swing leg) is moved from $[0.0, -0.05, 0]^T$ to $[0.12, -0.05, 0]^T$ and covered a distance of 0.12 m.

The amount of power consumed by i^{th} joint has been computed as the product of motor torque (τ_i) and angular velocity (\dot{q}_i). The amount of heat loss is also computed, and the average power consumption over a cycle of time period T is considered as the objective function P , as given in Eq. (32). Here, K is constant, and its value is assumed⁵² to be equal to 0.025. The single-objective optimization problem during SSP is mathematically stated as follows:

$$\text{Minimize } P = \sum_{i=1}^n \frac{1}{T} \int_0^T (|\tau_i \dot{q}_i| + K \tau_i^2) dt \quad (32)$$

subject to

$$q_{\min}^i \leq q_{\text{JointAngle}}^i \leq q_{\max}^i ,$$

$$\Delta \tau_{ij}^{\max} \leq 1.2 \text{ Nm} ,$$

$$X_{DBM}^{\min} > 0.0 \text{ m} ,$$

$$Y_{DBM}^{\min} > 0.0 \text{ m} ,$$

$$X_{DBM}^{\text{Avg}} \geq 0.05 \text{ m} ,$$

$$Y_{DBM}^{\text{Avg}} \geq 0.02 \text{ m} ,$$

and

$$0.25 \leq x_1 \leq 0.31 \text{ (m)};$$

$$-0.05 \leq x_2, x_3 \leq 0.05 \text{ (m/sec)};$$

$$0.001 \leq x_4, x_5 \leq 0.2 \text{ (m/sec)};$$

$$-0.2 \leq x_6, x_7 < 0.2 \text{ (m/sec)};$$

$$0.015 \leq x_8 \leq 0.030 \text{ (m)};$$

$$0.4 \leq x_9 \leq 4 \text{ (sec)};$$

where, x_1, x_2, \dots, x_9 are the decision variables,

$$q_{\min}^i = [-1.14, -0.38, -1.53, -0.09, -1.19, -0.39, -0.79, -1.53, -0.10, -1.18, -0.76]^T \text{ (rad)}$$

$$\text{and, } q_{\max}^i = [0.74, 0.79, 0.48, 2.11, 0.92, 0.76, 0.38, 0.48, 2.12, 0.93, 0.39]^T \text{ (rad)}$$

The parameter: x_1 represents hip height. x_2 and x_3 denote the initial and final velocities associated with the hip height, respectively. x_4 and x_5 represent the initial and final sagittal velocities, whereas x_6 and x_7 indicate the initial and final lateral velocities. x_8 and x_9 denote the maximum swing height and time spent in a SSP, respectively. q_{\min}^i and q_{\max}^i are the minimum and maximum joint rotations measured in *radian* for i^{th} joint (refer to Fig. 4). The first joint of q_i corresponds to *HipYawPitch* and other joints' values are counted for the left and right legs by following the order from the hip to ankle joint's angle limit. These values are taken from the official website⁴⁴.

A cycle time is divided into ten equal parts. Superscripts *min* and *Avg* represent the minimum DBM and Average DBM during cycle time. Combining both the constraints for DBM (minimum and average), the robot should never attain a zero DBM and maintain an average value either equal to or more than 50% of the maximum possible DBM. $\Delta \tau_{ij}^{\max}$ is the maximum possible torque fluctuation for i^{th} joint in j^{th} time interval. The lower and upper bounds for hip height are selected based on the reachable space by the robot without violating the joint limit constraints. The maximum hip height achievable with the stretched leg is 0.334 m; however, the robot could not move at this height. A suitable upper bound for hip height is considered, and the two more decision variables associated with it could further increase or decrease it without violating the joint limits. The NAO Devils Team from Germany achieved a maximum forward speed of 0.4447 m/sec in RoboCup 2010, as reported⁵³ in the literature, and the initial and final velocities are kept within this range. For the purposes of this study, the maximum swing height and single support time are specified as 0.030 m and 4 seconds, respectively.

4.2. Double support phase

A single-objective optimization problem for DSP is also formulated to minimize the power consumption (refer to Eq. (32)), when the torso shifts its position from the Left (previous support leg) to the Right Leg (next support leg). The positions of the left and right feet considered during DSP are $[0.06, 0.05, 0]^T$ and $[0.12, -0.05, 0]^T$, respectively. The hip is moved from position $[0.07, 0.025, Z_H]^T$ to $[0.11, -0.025, Z_H]^T$. The hip movement is in three-dimensional space, as in SSP. The single-objective optimization problem during DSP is defined as follows:

Minimize P (refer to Eq. (32))

subject to

$$\begin{aligned} q_{\min}^i &\leq q_{\text{JointAngle}}^i \leq q_{\max}^i \\ \Delta\tau_{ij}^{\max} &\leq 1.2 \text{ Nm} , \\ X_{DBM}^{\min} &> 0.0 \text{ m} , \\ Y_{DBM}^{\min} &> 0.0 \text{ m} , \\ X_{DBM}^{\text{Avg}} &\geq 0.08 \text{ m} , \\ Y_{DBM}^{\text{Avg}} &\geq 0.08 \text{ m} , \end{aligned}$$

and

$$\begin{aligned} 0.25 &\leq x_1 \leq 0.31 \text{ (m)}; \\ -0.05 &\leq x_2, x_3 \leq 0.05 \text{ (m/sec)}; \\ 0.001 &\leq x_4, x_5 \leq 0.2 \text{ (m/sec)}; \\ -0.2 &\leq x_6, x_7 \leq 0.2 \text{ (m/sec)}; \\ 0.2 &\leq x_8 \leq 2 \text{ (seconds)}; \end{aligned}$$

Here, x_1, x_2, \dots, x_8 are the decision variables. The parameters used here are the same as that of the already defined for the SSP case. However, here, x_8 represents time spent in DSP, and there is no swing height trajectory since both legs are on the ground. Moreover, the stability margin during DSP is expected to be more than that of SSP, so the constraints functions related to average DBM are modified accordingly. q_{\min}^i and q_{\max}^i are the minimum and maximum joint rotations possible for q^i joint, which was kept the same as that mentioned for SSP.

4.3. Constraints considered during the single and double support phase

We considered the following six functional constraints for single-objective optimization during SSP and DSP. The first two constraints are related to joint limits and torque fluctuation. The last four constraints are focused on the DBM.

- The joints should move within their allowable ranges. The violation of these constraints would affect the walking motion.
- The fluctuation of torque should be within the specified limit. The violation of these constraints means the robot needs a sudden torque requirement, which might affect the motion due to the motor's failure.
- The motion should be dynamically stable. It must maintain a positive DBM in the x and y directions during SSP and DSP in a cycle. The violation of these constraints affects the robot's stability and signifies that the robot is not balanced, at least in one-time intervals, despite maintaining the desired average balance margin.
- The Average DBM in the x and y directions should always be equal to or greater than 50% of the maximum possible stability margin during SSP. The Average DBM in both directions should be either equal to or greater than 0.08 m during DSP. Both DBM constraints will ensure dynamic stability throughout the motion.

5. Results and Discussion

Metaheuristic algorithms are employed to solve this optimization problem. PSO⁵⁴ is one of the most popular swarm-based evolutionary algorithms used for optimization. Each swarm consists of several particles, which search in n -dimensional space with different velocities. Each particle has the memory to track its current best position. As the generation progresses, it modifies its position by updating its velocity, while comparing it with the swarm's global best. The PSO algorithm in the MATLAB environment is obtained from Yarpiz-Academic Source Codes and Tutorials⁵⁵. The constant inertia weight, personal learning coefficient (cognitive parameter), and global learning coefficient (social parameter) are taken as 1, 1.5, and 2, respectively. The swarm size and the maximum number of iterations are considered as 50 and 200, respectively.

GA is another popular optimization technique for finding the optimum solution. Binary-coded GA is not suitable for representing large dimensions with continuous search space. Thus, an RCGA is used in this study to deal with the real

parameters. Several versions of RCGA are available in the literature with different crossover and mutation operators. Different versions of RCGA were used in this study, but RCGA consists of simulated binary crossover (SBX) ⁵⁶, and polynomial mutation ⁵⁷ is found to be more efficient. The generated solutions for the next iteration depend on the probability distribution, which was assumed to be polynomial in nature. The distribution indices for simulated binary crossover and polynomial mutation are taken as 2 and 20, respectively. A population size of 50 and 200 generations are considered to get an optimal solution.

The performance and optimal solutions obtained by both optimization algorithms are discussed separately for SSP and DSP. The optimal solutions obtained using PSO and GA are also evaluated to compute the constraints value and a few desirable parameters, as given in Tables 7 and 9 for SSP and DSP, respectively. For these two walking phases, the solutions obtained by PSO and GA are examined for their influences on power consumption. The PSO and GA solutions' improvement across the generations of gait parameters is utilized to find a relationship between power consumption and gait parameters.

Apart from that, the performance of algorithms is also compared over several runs. Eleven sets of the initial population were generated at random. Both GA and PSO are used to optimize separately using one set of the initial population. There are 11 sets of results for the GA and PSO, each from all 11 sets of the initial population. The GA and PSO are started from the same initial population in each run. Their median performance is recorded to give equal opportunity to both algorithms to find a better solution. The population's 5th and 7th initial sets are found to be responsible for the median performance during SSP and DSP, respectively. These optimal solutions are reported in Tables 6 and 8 for SSP and DSP, respectively. The SSP and DSP are analyzed separately to study the effects of hip height, swing height, and terminal velocities in sagittal and lateral planes. PSO is found to be marginally better than the GA during SSP and DSP.

5.1. Single support phase

As explained above, GA and PSO algorithms are used to run with 11 sets of initial populations selected at random. These initial sets are found to give the best to worst performance (based on the final value of the objective function) using GA and PSO. Both the GA and PSO are found to yield the median performance for the 5th set of the initial population. Table 6 shows the optimal solutions for SSP using PSO and GA for the median performance from the 5th set of the initial population.

Table 6. The outcome of the single objective optimization (in SSP)

Decision variables	Optimal value using PSO	Optimal value using GA
x_1 (m)	0.31	0.31
x_2 (m/sec)	-0.0020	-0.005
x_3 (m/sec)	0.0034	0.000
x_4 (m/sec)	0.0080	0.0031
x_5 (m/sec)	0.0025	0.0017
x_6 (m/sec)	0.0243	0.0364
x_7 (m/sec)	-0.0256	-0.0135
x_8 (m)	0.015	0.015
x_9 (sec)	4	4

Total average power consumption obtained using PSO and GA (median performance) is seen to be equal to 1.283 W and 1.303 W, respectively. Since there are 11 runs of each GA and PSO, the best value obtained in each generation was stored. We can further calculate three more values from these 11 sets of GA and PSO in each generation, viz. minimum of the best (*minBest*), average of the best (*AvgBest*), maximum of the best (*maxBest*). These three values obtained from each algorithm's best values over the generations, namely the minimum, average, and maximum of the best, provided a lot of information on its dynamics. Figs. 9 (a) and (b) show the best performance of the PSO and GA over the generations.

The PSO is found to be better than GA because even for starting with the different initial populations, it has been successful in finding the same globally optimum solution. The PSO is found to perform marginally better than GA, due to being a better tool for both the local and global searches during optimization. However, GA got the better average very near to the minimum of the best optimal solution in each generation, but its error base with the maximum and minimum of the best values is significant compared to PSO. It is not found to be as good as the PSO, as it needs to be run multiple times to get the globally optimum solution. The optimal solutions obtained by both the algorithms slightly vary in sagittal and lateral velocities (refer to Table 6), which showed that there could be more combinations of connecting velocities during

an exchange of phases and still consume a similar amount of power. A study of these optimal solutions for power consumption would provide more information.

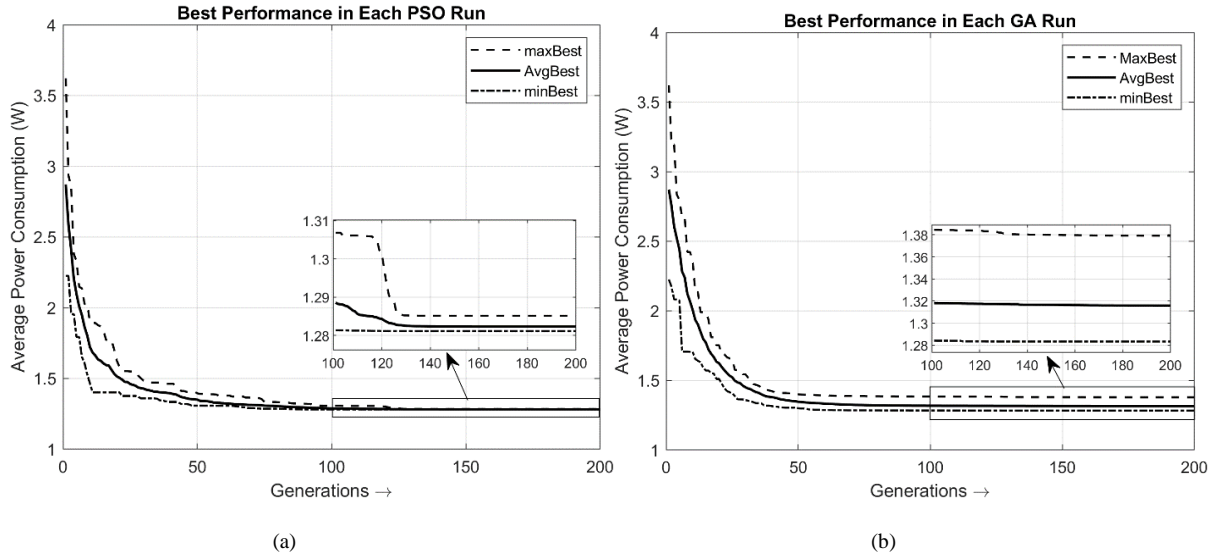


Fig. 9. The maximum of the best, average of the best, and a minimum of the best of the objective function in each generation obtained by (a) PSO and the (b) GA during the 11 runs in SSP.

5.1.1. Comparison of the obtained optimal solutions based on the performance metrics

The final optimal solutions obtained from PSO and GA are compared based on six defined performance indices (other than fitness function). The constraint functions and maximum swing height are considered as a way to measure the effectiveness and quality of the optimal solution.

Table 7. Comparison of the result based on the performance index (in SSP)

Sr. No.	Performance Index	Algorithm	
		PSO	GA
1	$\Delta\tau^{max} (Nm)$	0.4492	0.5143
2	$X_{DBM}^{min} (m)$	0.0307	0.0308
3	$Y_{DBM}^{min} (m)$	0.0085	0.0084
4	$X_{DBM}^{Avg} (m)$	0.0641	0.0591
5	$Y_{DBM}^{Avg} (m)$	0.0200	0.0200
Maximum swing height Achieved ($S_h^{max} m$)		Average Power Consumption (W)	
6	0.015	1.283	1.303
7	0.018	1.292	1.333
8	0.022	1.308	1.439
9	0.024	1.317	1.667
10	0.026	1.588	2.605
11	0.028	2.453	3.152

$\Delta\tau^{max}$ denotes the maximum change in torque recorded for any joint in any given interval. This value should be as low as possible. The optimal PSO-solution reduced the torque fluctuation by nearly 13% compared to the optimal GA-solution. The minimum DBM in the x and y directions are very close to each other. However, PSO is able to get a better average of DBM in the x -direction by 5 mm compared to that of the GA. Serial numbers 6-11 in Table 7 list the amount of average power required to achieve certain maximum swing heights determined by the potential solutions of PSO and GA, respectively. It is worth noting that PSO outperformed GA in terms of identifying the best combination of decision variables, resulting in reduced power consumption for comparable swing height. One of the interesting things to note here that PSO solution can achieve a maximum swing height of 0.024 m while consuming only 1.317 W (refer to Fig. 13), which is only 2.6% higher than the optimal one. The power consumption yielded by the GA is seen to be 26.57% higher

than that obtained by the PSO for reaching the same swing height. A detailed discussion related to the effect of higher swing height on power consumption is carried out in section 5.1.5.

PSO found the walking trajectories that offered the higher swing height while consuming a similar amount of power, enabling the robot to avoid obstacles without extra power consumption. The optimal solution found by PSO has also minimized the torque fluctuations while providing an improved stability margin compared to GA. Thus, the PSO solutions are superior and proved their effectiveness during the optimization compared to that of the GA during SSP.

5.1.2. Effect of hip motion on power consumption

Power consumption is reduced with an increase in hip height. The leg gets straighter with the higher hip height, and the joint angles' variations are less, directly affecting the torque variation and angular velocity. The knee joint⁵⁸ is considered the primary source of energy consumption. There is less torque demand at knee joints due to the higher hip height, reducing overall power consumption. The design variables: x_1 , x_2 and x_3 are responsible for the trajectory of hip vertical motion. Fig. 10 shows these decision variables' variations with respect to objective function using PSO (left) and GA (right). Omran et al.⁵⁹ studied the effect of the vertical motion of the CoM on energy consumption and reported a natural up/down oscillation of CoM that resulted into a reduction in torque. Mandava and Vundavilli⁶⁰ found that the straight hip trajectory has a better stability margin than the cubic polynomial trajectory. Minimum power consumption and maximum stability margin required different vertical motions of CoM. The optimization algorithm found the minimum average power consumption without violating the stability margin. Both PSO and GA provided more solutions for negative x_2 and positive x_3 velocity, which will generate a negative slope for the hip trajectory. Solutions provided by GA and PSO are in a very close interval, and those values are less than ± 0.005 m/sec, which signifies nearly a straight line trajectory with variation within a few mm. It is also observed that a higher stability margin is available with the lower CoM. The hip travels closer to the ground to lower the CoM, thereby increasing stability and preventing the violation of stability constraints. The solution provided by PSO is better due to the low variation of hip trajectory compared to GA. As explained in section 5.1.1, the PSO solution is able to find a better average of X_{DBM} for similar average power consumption.

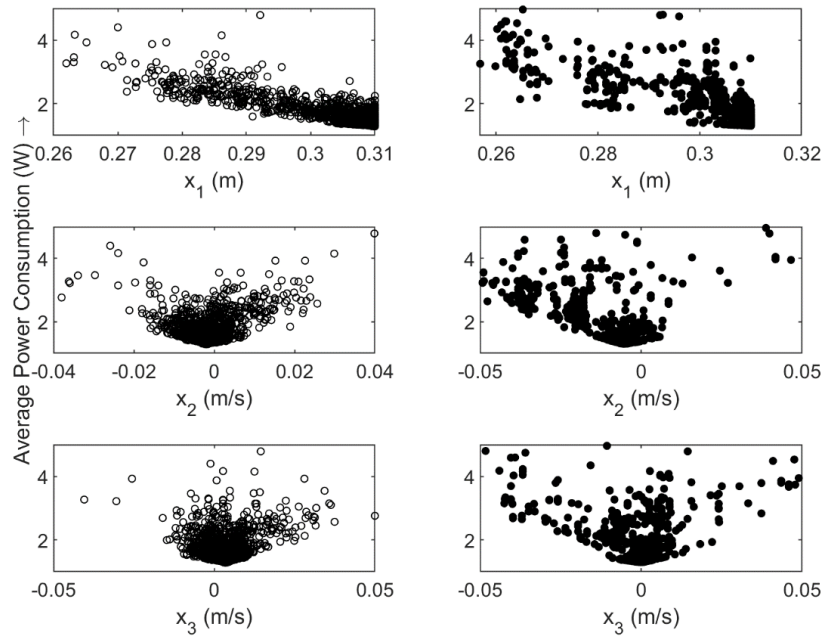


Fig. 10. Variations of the objective function with hip height (x_1), initial velocity (x_2) and final velocity (x_3) of hip height, as shown for all the feasible solutions obtained using PSO (left) and GA (right) (in SSP).

5.1.3. Effects of initial and final forward velocities on power consumption

Fig. 11 shows the variations for sagittal velocities obtained using PSO and GA. The initial and final sagittal velocities help in connecting the previous and next walking phases, respectively. It is assumed that the robot's initial sagittal velocity in SSP is received from DSP, and the final sagittal velocity in SSP would be transferred to the next DSP. PSO and GA provided the initial and final velocities ranging from 0.002 to 0.008 m/sec. Initial and final velocities beyond this range

introduce sudden acceleration to the robot, leading to increased torque requirements and, consequently, higher power consumption.

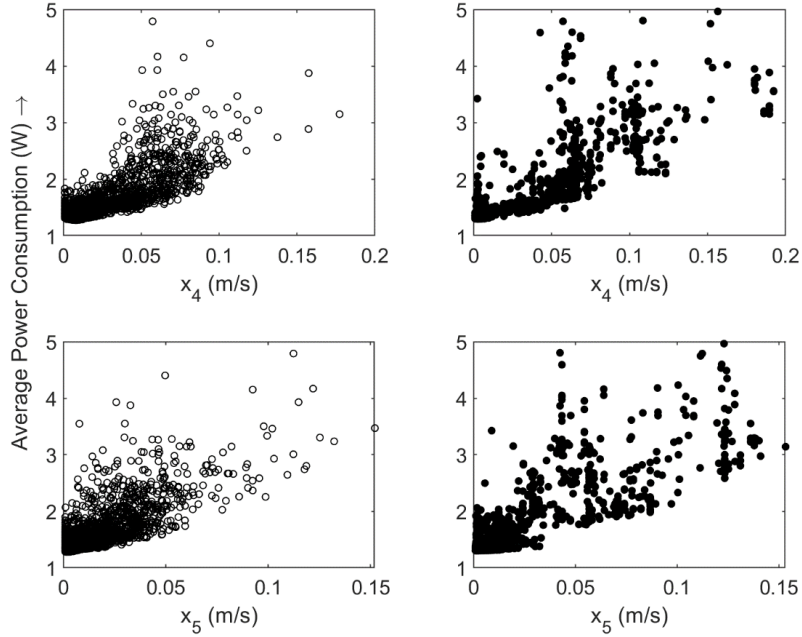


Fig. 11. Variations of the objective function with initial (x_4), and final (x_5) sagittal velocities, as shown for all the feasible solutions obtained using PSO (left) and GA (right) (in SSP).

5.1.4. Effects of initial and final lateral velocities on power consumption

Upper body movement in the lateral direction plays an important role in balancing the robot. A higher value in the robot's lateral velocity increases the power consumption due to higher acceleration. However, an optimal value is required to ensure the desired dynamic balance. Once the robot enters into SSP, the upper body should stay there for some time while helping the movement in x direction. At the end, it moves back towards the middle of the legs, signaling the start of the DSP. $y = 0.025$ is the point from which the upper body entered into SSP, and it should bring itself at the same point fulfilling all the constraints.

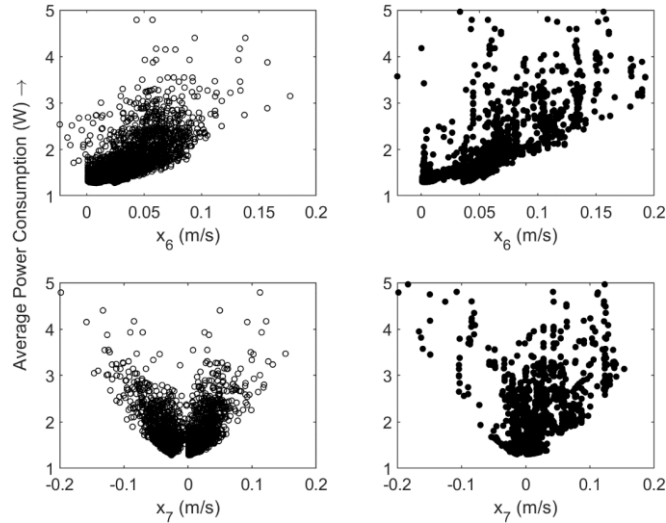


Fig. 12. Variations of the objective function with initial (x_6), and final (x_7) lateral velocities, as shown for all the feasible solutions obtained using PSO (left) and GA (right) (in SSP).

A positive and negative velocity will help the robot to swing at the right time to change direction. PSO has provided nearly equal initial and final lateral velocities, which can be utilized to connect other phases smoothly. Though an initial and final

velocity during SSP and DSP cannot guarantee the nature of the velocity profile during walking, it can be used to connect two different phases to avoid any jerky motion during the exchange. The same velocity while entering and exiting from SSP or DSP helps in switching the walking phases better. Fig. 12 shows these variations of the design variables as obtained from PSO and GA. An increase in these velocities would increase power consumption. There is a limited range of lateral velocities for the minimum power consumption, and due to this fact that the initial and final hip locations at switching points are kept fixed. Only lateral velocities could prevent the violation of the stability margin. The higher stability margin in the y-direction depends on these two velocities.

5.1.5. Effect of Swing leg height on power consumption

Swing height helps in avoiding collisions with obstacles and allows larger step sizes. Fig. 13 shows the swing leg height variations obtained using PSO and GA over the generations. GA found the walking trajectories that raised the swing height up to 2 mm for nearly the same power consumption. At the same time, this range is seen to be substantially higher, up to 9 mm, in the case of solutions provided by PSO. As discussed in section 5.1.1, serial numbers 6-11 in Table 7 provide information on average power consumption against the swing height. This also exhibits the effectiveness of solutions provided by each algorithm on the achieved swing height.

PSO is better at finding the combination of all the decision variables to consume nearly the same power for the higher swing leg. Moreover, similar power consumption for a slightly higher swing height is due to the fixed step length. It was also reported that most of the work is done at the hip joint⁶¹ related to power consumption. Most of the power consumption by hip joints is utilized in swinging the leg from the initial to the final positions, whereas the height is maintained by the swing leg's knee and ankle pitch joint. However, a high swing height generally consumes more power beyond these ranges, as the swing leg's ankle and hip pitch must be adjusted to help track the swing leg trajectory. When the decision variables: sagittal and lateral velocities, are combined with hip trajectory, a new walking trajectory is created that allows a higher step height. Here, PSO is able to find better solutions compared to that of the GA, in this case.

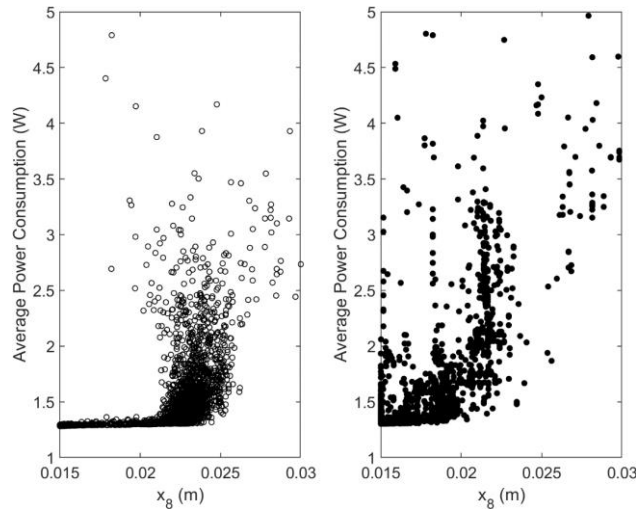


Fig. 13. Variations of the objective function with maximum height (x_g) achieved by swing leg, as shown for all the feasible solutions obtained using PSO (left) and GA (right) (in SSP).

5.1.6. Effect of time spent in single support phase on power consumption

Fig. 14 shows the variation of the objective function with time spent in SSP for all the feasible solutions obtained using PSO (left) and GA (right). The optimal power consumption is mostly dependent on the average speed, which can be calculated as the ratio of distance covered in a walking phase to the elapsed time. The distance is kept constant, and the power consumption depends on the time spent in SSP. A higher time spent in SSP signifies a slower speed, and it is evident that the robot is consuming less power at a slow pace, as shown in Fig. 14. However, an extremely slow speed adversely affects the dynamic stability. Both algorithms have shown similar trends. The power could be seen increasing exponentially with a shorter duration. The angular velocity and torque both got increased, which affected the power consumption.

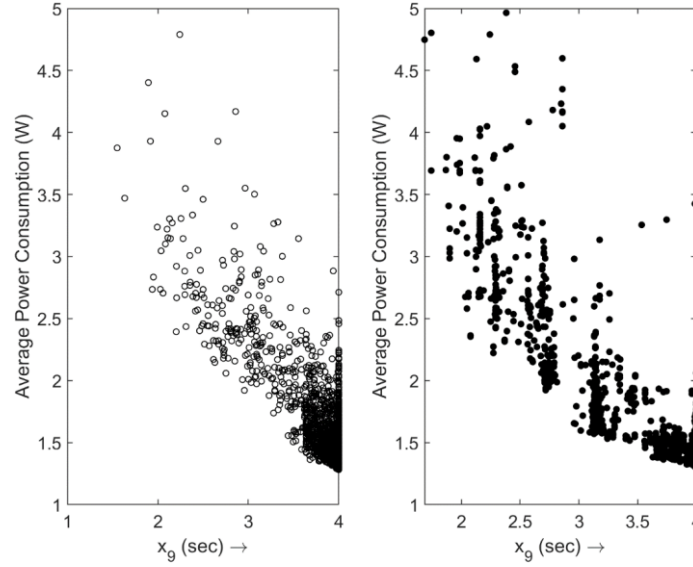


Fig. 14. Variations of the objective function with time spent (x_9) in single support phase, as shown for all the feasible solutions obtained using PSO (left) and GA (right) (in SSP).

5.2. Double support phase

The total average power consumptions obtained using PSO and GA are found to be equal to 1.0682 W and 1.0685 W, respectively. The outcome of single-objective optimization with the decision variable during DSP is given in Table 8. These algorithms could find the different combinations of sagittal and lateral velocities for similar power consumption. Power consumption is mostly affected by the average speed of the robot. Both the algorithms provided similar results, but PSO is seen to perform marginally better than GA during DSP. The effects of various decision parameters on power consumption have been discussed below. Similar to SSP, during DSP also, both PSO and GA are run 11 times using eleven sets of the initial population. The best performance analysis of both algorithms is done in a similar way, as reported for SSP. Fig. 15 compares the average of the best collection with the minimum and maximum of best values in each generation for both algorithms during eleven run samples. PSO and GA both converge to nearly similar values. However, the PSO is able to perform better in each run compared to GA due to its low error base with the maximum and minimum of best values. The optimal solutions yielded by the two algorithms are also found to be very similar. It also proved that considering the DSP into two SSPs reduces the complexity, and both algorithms could quickly converge to find the globally optimal solution.

Table 8. The outcome of the Single Objective Optimization (in DSP)

Decision variables	Optimal value using	
	PSO	GA
x_1 (m)	0.3100	0.3100
x_2 (m/sec)	-0.0008	0.0002
x_3 (m/sec)	-0.0055	-0.0052
x_4 (m/sec)	0.0520	0.0582
x_5 (m/sec)	0.0010	0.0010
x_6 (m/sec)	-0.0367	-0.0384
x_7 (m/sec)	-0.0424	-0.0405
x_8 (sec)	2	2

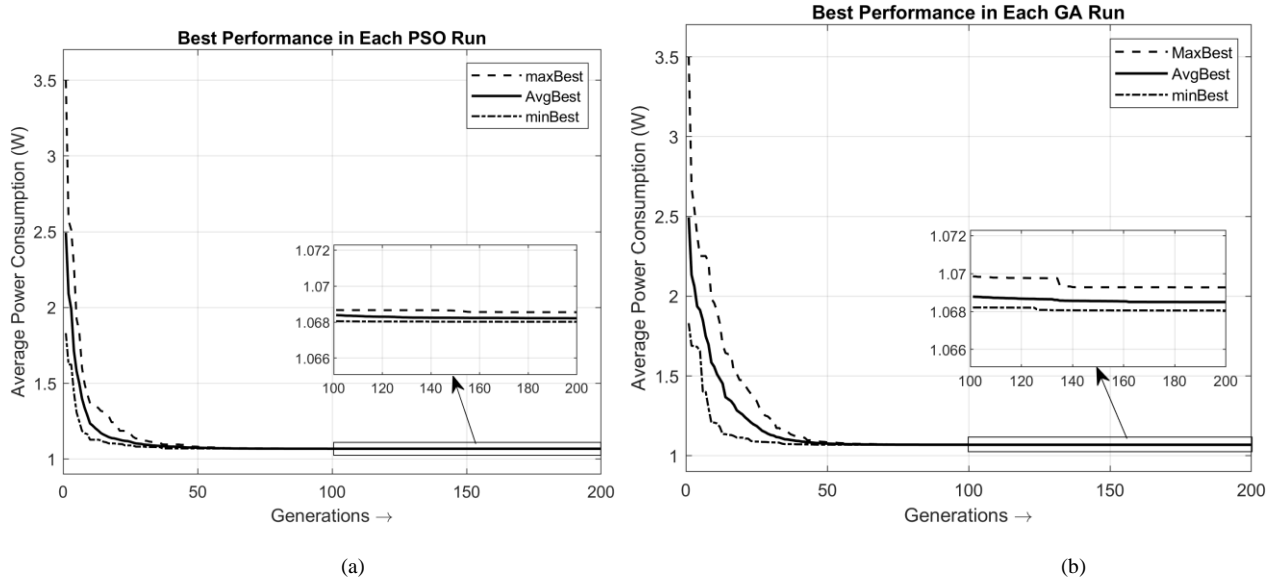


Fig. 15. The maximum of best, average of best, and minimum of best of the objective function in each generation obtained by (a) PSO and (b) GA during 11 runs (in DSP).

5.2.1. Comparison of the obtained optimal solutions based on the performance metrics

Table 9 lists all the values of the performance index as obtained from the final optimal solutions of each algorithm. As evident from the above discussion, both PSO and GA are found to give very similar results, as seen in the table below. The performance indices consisting of the constraints' values are very close for both algorithms. Though the PSO has given marginally better average power consumption, the GA is able to provide a much better value in terms of low fluctuation of torque ($\Delta\tau^{max}$) and slightly higher average DBM in the x and y direction compared to PSO. PSO provided a better minimum value of the DBM in the x and y directions. GA solution is found to have a lower torque change and a higher average DBM at the cost of a minor increase in power consumption. GA is able to reduce the change in torque by 3% compared to PSO. GA is also able to improve the average DBM in the x and y -directions, nearly by 0.2 mm. This also shows that PSO and GA could minimize the power consumption without violating any constraints; however, GA is able to provide a similar power consumption but with better values in the performance index. The importance of GA in finding the optimal solution related to the walking trajectories of biped robots cannot be neglected.

Table 9. Comparison of the result based on the performance index (in DSP)

Sr. No.	Performance Index	Algorithm	
		PSO	GA
1 ^a	$\Delta\tau^{max}$ (Nm)	0.6751	0.6554
2 ^b	X_{DBM}^{min} (m)	0.0734	0.0731
3 ^b	Y_{DBM}^{min} (m)	0.0700	0.0699
4 ^b	X_{DBM}^{Avg} (m)	0.0926	0.0928
5 ^b	Y_{DBM}^{Avg} (m)	0.0809	0.0811
7 ^a	Avg Power Consumption (W)	1.0682	1.0685

^aLower the better. ^bHigher the better

5.2.2. Effect of hip motion on the power consumption

A higher hip height consumes less energy for the reasons that were explained earlier. However, a much larger support area is available during DSP; therefore, a wide range of initial and final velocities can be seen in Fig. 16. The robot has utilized a positive initial velocity to increase its height to further reduce power consumption without violating any constraints. Both PSO and GA are able to find similar values related to hip height parameters. Fig.16 shows the variations of the solutions, as obtained from PSO and GA. A similar trend is also observed in Farzadpour *et al.*⁶² during the study of DSP.

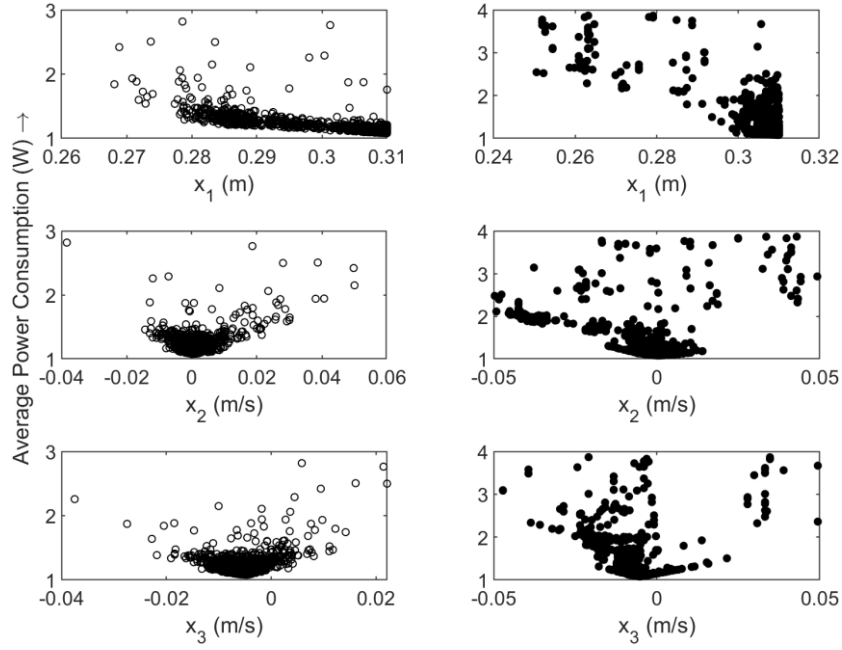


Fig. 16. Variations of the objective function with hip height (x_1), initial velocity (x_2) and final velocity (x_3) of hip height, as shown for all the feasible solutions obtained using PSO (left) and GA (right) (in DSP).

5.2.3. Effect of initial and final forward velocities on power consumption

Fig. 17 shows the variations of sagittal velocities using PSO and GA. A much higher velocity range is obtained in DSP than that of SSP because of the larger support polygon. In DSP, the initial sagittal velocities for both algorithms varied from nearly 0.045 to 0.075 m/sec, whereas the final velocity varied from 0.001 to 0.02 m/sec. It shows that the wide ranges of walking speeds are available during DSP to connect an SSP. Despite different terminal velocities, the robot is able to consume a similar amount of power because power is mainly dependent on the average speed of the robot in that phase.

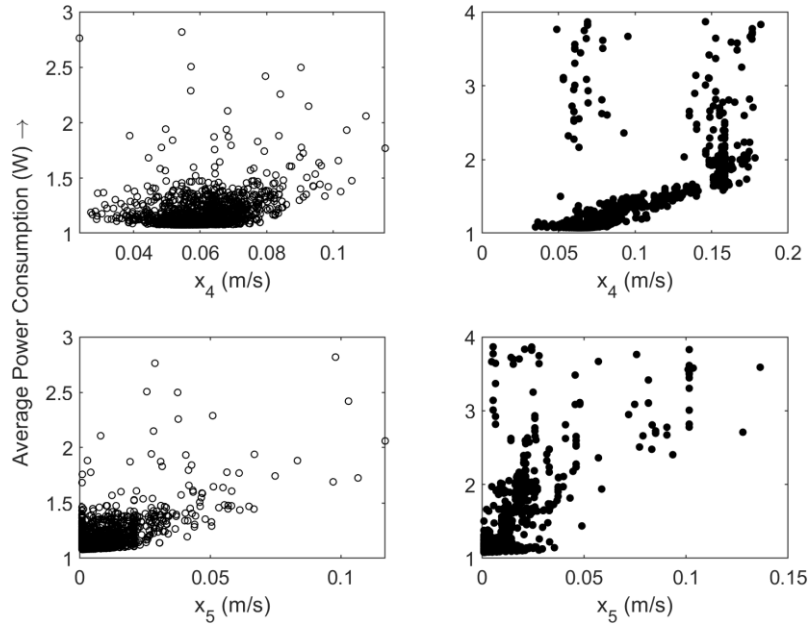


Fig. 17. Variations of the objective function with initial (x_4), and final (x_5) sagittal velocities, as shown for all the feasible solutions obtained using PSO (left) and GA (right) (in DSP).

5.2.4. Effect of initial and final lateral velocities on power consumption

In DSP, the robot needs to travel from a positive y-direction to a negative y-direction, and thus, both initial and final velocities need to be negative. It is interesting to note that initial and final velocities obtained from both algorithms are varied from -0.035 m/sec to -0.075 m/sec, as shown in Fig 18. A similar value of initial and final velocities will help in connecting the previous and next walking phases smoothly. The lower initial velocity did not satisfy the stability constraints; thus, there is a less feasible solution near zero. Beyond the given ranges, the higher-end velocities consumed more power due to the higher acceleration. A few feasible solutions are found to exist with positive velocity but at higher power consumption. Positive velocity helps to attain a new position, and then, the velocity could be changed to move from one support leg to another.

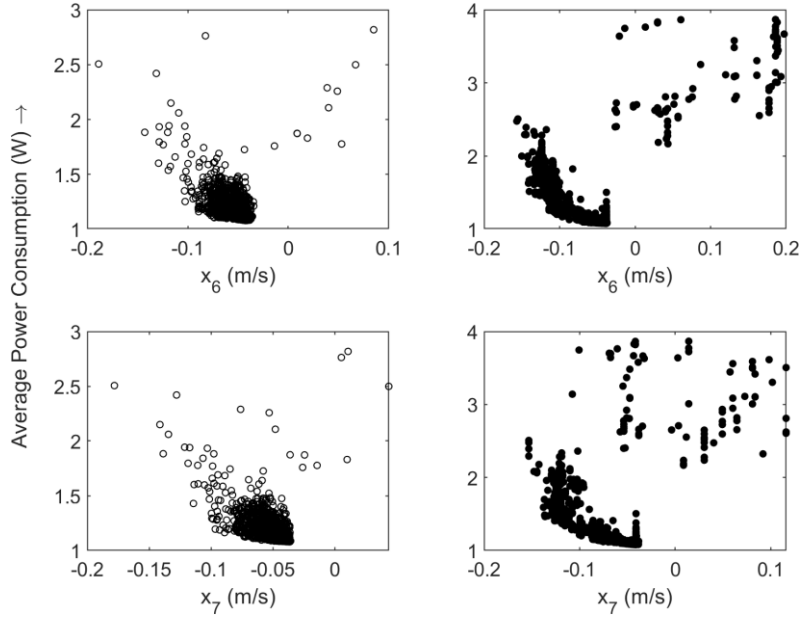


Fig. 18. Variations of the objective function with initial (x_6), and final (x_7) lateral velocities, as shown for all the feasible solutions obtained using PSO (left) and GA (right) (in DSP).

5.2.5. Effect of time spent in double support phase on power consumption

The DSP is also more energy efficient at a slower speed, as evident from Fig. 19.

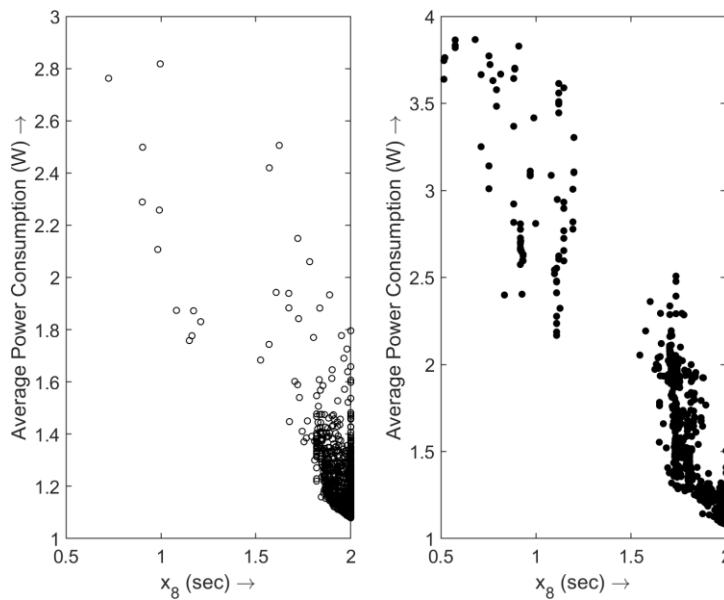


Fig. 19. Variations of the objective function with time spent (x_8) in double support phase, as shown for all the feasible solutions obtained using PSO (left) and GA (right) (in DSP).

A reduction in time spent in the DSP is more costly in power consumption, as it increases the average speed. Available solutions having a shorter duration could be selected if speed is the main criterion at the higher power consumption. One of the most intriguing aspects is the fact that there is a discontinuity in the solutions between some durations. The desired average stability margin constraint has been found to be violated for those periods due to the changes in trajectory. It is also observed that the robot's stability margin got reduced when it walked too quickly or too slowly. The robot's average speed also influences the desired DBM.

5.3. Statistical Analysis

A Wilcoxon rank-sum test is carried out in addition to the performance analysis to declare the better algorithm out of these two. PSO is found to give better performance than GA during both the SSP and DSP of the humanoid robot. The statistical analysis is carried out using MATLAB.

5.3.1. Single support phase

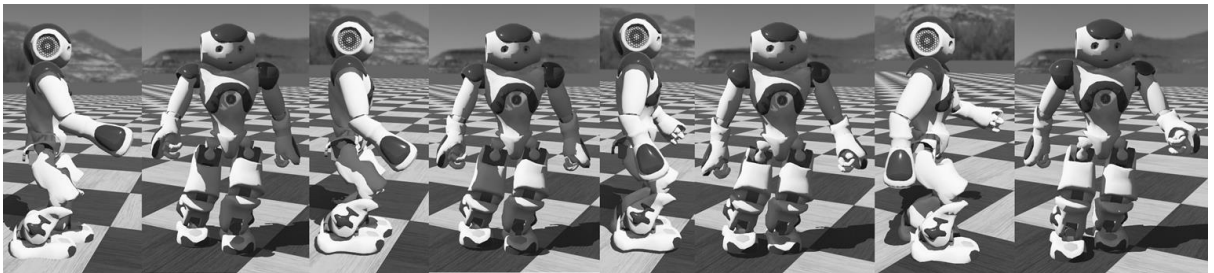
Two sets of GA and PSO fitness values (each consisting of eleven values) obtained at the final generation are used to perform the Wilcoxon rank-sum test in MATLAB. The rank-sum test produced a p-value equal to 0.000235. Since the p-value is less than 0.05, there is enough evidence to reject the null hypothesis that PSO will turn out to be better than GA during SSP with a 5% significance level. Moreover, a left-sided test is also performed to assess the decrease in the median of PSO compared to GA at the 5% significance value. Both the p-value (0.000117) and the result of the hypothesis (was true) indicated the rejection of the null hypothesis of equal medians at the default 5% significance level. The rank-sum test statistic and z-statistic are found to be equal to 70 and -3.6772 , respectively. This left-tailed alternative hypothesis further stated that the median of PSO is less than the median of GA during SSP.

5.3.2. Double support phase

Wilcoxon rank-sum tests is also performed for DSP using eleven values of PSO and GA fitness values obtained at the final generation. The p-value obtained from the rank-sum test is seen to be equal to 0.0181. There is also enough evidence to reject the null hypothesis that PSO will be better than GA during DSP with a 5% significance level. The p-value (0.0181) and the result of the hypothesis (was true) in a left-tailed, alternative hypothesis indicated the rejection of the null hypothesis of equal medians at the 5% significance level. The values of the rank-sum test statistic and z-statistic are found to be 90 and -2.3639 , respectively. These values confirm that the median of PSO is less than that of GA during DSP.

5.4. Simulation Results

A simulation is performed on the NAO humanoid robot in the Webots simulator. NAO is commanded to walk on the planned optimal hip, swing leg, and hand motion trajectory. The joint angles obtained using IK are written in a motion file, and each line corresponding to the next step is executed for each 40 ms. This is comparable with the functions provided by Softbank Robotics and will show a similar result if executed on the actual NAO robot. The robot is able to walk without falling on the ground, which confirms that it is stable and does not violate any joint limit. The Webots simulator verified the optimal solution provided by PSO and GA for SSP and DSP. However, Figs. 20 (a) and (b) show the simulations for SSP and DSP, respectively, according to the optimal solution provided by PSO.



(a)

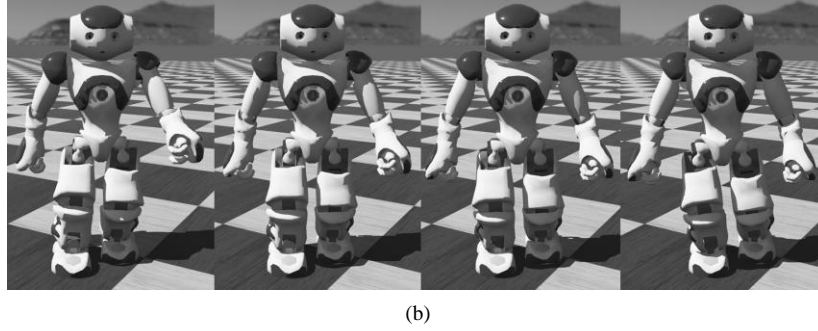


Fig. 20. *a)* Front and side views at each 1 second during SSP, *b)* Front view at every 0.25 seconds during DSP of NAO robot (from left to right) shown as captured from the Webots simulator.

6. Concluding Remarks

This study has found optimal gait parameters for consuming minimum power for NAO biped robot for SSP and DSP, separately, while walking on an even floor after maintaining a high DBM. NAO robot's hip movements are allowed in x , y , and z directions. Constrained optimization problems have been solved using PSO and GA for both phases, *viz.*, SSP and DSP separately. Joint limits violation and maximum allowable torque fluctuations have also been considered as constraints to avoid motor failure. The maximum allowed torque change has ensured smoothness at the torque level to lower the power consumption. After analyzing the optimal solutions, it has been found that the higher hip height helps to minimize power consumption by relieving the extra load from the ankle and knee joints. In contrast, a lower hip height has improved stability. A lower hip height brings the CoM of the robot closer to the ground, thus, affecting the dynamic stability. Robots walking at a slow speed with high hip height and low swing height would consume less power due to the lowest possible joint variation. The more time spent in a walking phase has helped the robot to move slowly and, thus, reduced the power consumption but at the cost of poor stability. During SSP and DSP, a natural oscillation of hip trajectory minimizes torque, but a straight hip trajectory closer to the ground has an enhanced stability margin. Thus, minimum power consumption and maximum DBM have been found to contradict each other.

The robot can take the higher speed in DSP due to its larger support polygon, preventing falling. It has also been observed that the DBM could be significantly improved by suitable arms' movement during SSP and DSP. Different sagittal and lateral velocities were available, but the optimal power consumption has mostly dependent on the average speed during a single or double support phase. Due to its larger support polygon, there were higher ranges of terminal velocities available during DSP. DSP should not be neglected because it is essential in maintaining steady locomotion, especially while walking at a moderate speed. In comparison to SSP, DSP has provided stability in a biped model over a large range of walking speeds. DBM has also been found to be directly affected by the average speed of the robot during SSP and DSP. An extremely fast or very slow-paced robot will have a poor stability margin. The findings of this study are in tune with the general experience of a human being walking on plain ground.

The proposed work was also simulated in a suitable environment using *Webots* simulator to confirm its effectiveness. Wilcoxon rank-sum test was performed using the two sets of samples (each set consists of eleven fitness values) obtained using PSO and GA at their final generation during SSP and DSP. The p -values were less than 0.05 in SSP and DSP to reject the null hypothesis that PSO is statistically significant in both cases. Moreover, a left-tailed, alternative hypothesis based on obtained p -value and the result of the hypothesis has indicated the rejection of the null hypothesis of equal medians at the 5% significance level. This confirms that the median of PSO is less than the median of GA during SSP and DSP. The PSO found the minimum power consumption during SSP and offered a better value in the performance index, which was defined based on the constraint functions and swing height. PSO solution has found the minimum torque change within the time interval, better average stability margin, and maximum height achieved by the swing leg for nearly similar power consumption. Though PSO was able to find the globally optimum value for power consumption during DSP, GA has provided marginally better torque fluctuation as compared to PSO. The PSO algorithm has been found to be better than GA due to its capability to search both globally and locally. The GA is better known for finding an optimal global solution.

The optimal solution of a single-objective optimization problem has mainly depended on the space of the design variable, and the minimum values have been found using a different combination of these variables. However, there might be a need for more stability or speed, and then a multi-objective optimization problem could be formulated to optimize the power and dynamic stability margin. A multi-objective optimization problem to minimize power and maximize DBM will be formulated and studied in the future to allow a designer to choose a suitable solution depending on the need. Cubic

polynomial trajectories for hip motion have been utilized in this study. However, other trajectories can also be tried for the hip motion in 3D space, and its impacts on DBM and power consumption will be studied in the future. The constraints like maximum and minimum joint rotations possible have been considered here. However, the maximum and minimum angular velocities and acceleration can also be considered and have been kept in the scope for future study. This work aimed to obtain the optimal gait parameters and study its effect on power consumption for the humanoid robot's motion in SSP and DSP separately. However, a continuous exchange of these phases for the robot's motion can be considered and has been kept in the scope of future studies.

References

1. X. Mu and Q. Wu, A complete dynamic model of five-link bipedal walking, in *Proceedings of the 2003 American Control Conference, 2003.* (2003), pp. 4926–4931.
2. R. Rajendra and D. Kumar Pratihara, Analysis of double support phase of biped robot and multi-objective optimization using genetic algorithm and particle swarm optimization algorithm, *S⁺ Adhara* **40** (2015) 549–575.
3. N. Kofinas, E. Orfanoudakis and M. G. Lagoudakis, Complete Analytical Forward and Inverse Kinematics for the NAO Humanoid Robot, *Journal of Intelligent and Robotic Systems: Theory and Applications* **77** (2014) 251–264.
4. E. Hashemi and M. Ghaffari Jadidi, Dynamic modeling and control study of the nao biped robot with improved trajectory planning, *Advanced Structured Materials* **16** (2012) 671–688.
5. E. Hashemi and A. Khajepour, Kinematic and three-dimensional dynamic modeling of a biped robot, *Proceedings of the Institution of Mechanical Engineers, Part K: Journal of Multi-Body Dynamics* **231** (2017) 57–73.
6. M. Alibeigi, S. Rabiee and M. N. Ahmadabadi, Inverse Kinematics Based Human Mimicking System using Skeletal Tracking Technology, *J Intell Robot Syst* **85** (2017) 27–45.
7. S. Sakka, L. P. Poubel and D. Cehajic, Tasks prioritization for whole-body realtime imitation of human motion by humanoid robots, in *Digital Intelligence (DI2014)* (2014), pp. 1–5.
8. F. Wang, C. Tang, Y. Ou and Y. Xu, A real-time human imitation system, in *Proceedings of the 10th World Congress on Intelligent Control and Automation* (2012), pp. 3692–3697.
9. X. Lv, J. Chai and S. Xia, Data-driven inverse dynamics for human motion, *ACM Trans Graph* **35** (2016), pp 1–12.
10. C. Hernández-Santos, R. Soto and E. Rodríguez, Design and dynamic modeling of humanoid biped robot e-robot, in *Proceedings - 2011 IEEE Electronics, Robotics and Automotive Mechanics Conference, CERMA 2011* (2011), pp. 191–196.
11. E. Kljuno and R. L. Williams, Humanoid Walking Robot: Modeling, Inverse Dynamics, and Gain Scheduling Control, *Journal of Robotics* **2010** (2010) 1–19.
12. C. Hernández-Santos, E. Rodríguez-Leal, R. Soto and J. L. Gordillo, Kinematics and dynamics of a new 16 DOF humanoid biped robot with active toe joint, *Int J Adv Robot Syst* **9** (2012) 190.
13. M. Rameez and L. A. Khan, Modeling and dynamic analysis of the biped robot, in *ICCAS 2015 - 2015 15th International Conference on Control, Automation and Systems, Proceedings* (2015), pp. 1149–1153.
14. A. K. Kashyap, D. R. Parhi and S. Kumar, Dynamic Stabilization of NAO Humanoid Robot Based on Whole-Body Control with Simulated Annealing, *International Journal of Humanoid Robotics* **17** (2020).
15. X. Bajrami, A. Dermaku, A. Shala and R. Likaj, Kinematics and dynamics modelling of the biped robot, *IFAC Proceedings Volumes (IFAC-PapersOnline)* **46** (2013) 69–73.
16. M. Folgheraiter and B. Aubakir, Design and Modeling of a Lightweight and Low Power Consumption Full-Scale Biped Robot, *International Journal of Humanoid Robotics* **15** (2018), pp 1850022(1)-1850022(32).
17. M. Khadiv, M. Ezati and S. A. A. Moosavian, A Computationally Efficient Inverse Dynamics Solution Based on Virtual Work Principle for Biped Robots, *Iranian Journal of Science and Technology - Transactions of Mechanical Engineering* **43** (2019) 37–52.
18. S. Kajita and K. Tani, Study of dynamic biped locomotion on rugged terrain-derivation and application of the linear inverted pendulum mode, in *Proceedings. 1991 IEEE International Conference on Robotics and Automation* pp. 1405–1411.
19. M. Vukobratović and B. Borovac, Zero-moment point—thirty five years of its life, *International Journal of Humanoid Robotics* **1** (2004) 157–173.
20. Y. J. Seo and Y. S. Yoon, Design of a Robust Dynamic Gait of the Biped Using the Concept of Dynamic Stability Margin, *Robotica* **13** (1995) 461–468.
21. H. J. Chung, J. H. Kim and Y. Xiang, Rate of angular momentum in ZMP using efficient DH-based recursive lagrangian, *International Journal of Humanoid Robotics* **15** (2018).

22. Changjiu Zhou, Pik Kong Yue, Jun Ni and Shan-Ben Chan, Dynamically stable gait planning for a humanoid robot to climb sloping surface, in *IEEE Conference on Robotics, Automation and Mechatronics, 2004*. (IEEE, 2004), pp. 341–346.
23. J. Liu and O. Urbann, Bipedal walking with dynamic balance that involves three-dimensional upper body motion, *Rob Auton Syst* **77** (2016) 39–54.
24. D. Gong, J. Yan and G. Zuo, A Review of Gait Optimization Based on Evolutionary Computation, *Applied Computational Intelligence and Soft Computing* **2010** (2010) 1–12.
25. D.K. Pratihar, *Fundamentals of Robotics*, 1st ed., Narosa Publishing House Pvt. Ltd., New Delhi, India, 2017.
26. Tushar, P. R. Vundavilli and D. K. Pratihar, Dynamically balanced ascending gait generation of a biped robot negotiating staircase, in *IEEE Region 10 Colloquium and 3rd International Conference on Industrial and Information Systems, ICIIS 2008* (IEEE, 2008), pp. 1–6.
27. P. R. Vundavilli, S. K. Sahu and D. K. Pratihar, Online dynamically balanced ascending and descending gait generations of a biped robot using soft computing, *International Journal of Humanoid Robotics* **4** (2007) 777–814.
28. P. R. Vundavilli, S. K. Sahu and D. K. Pratihar, Dynamically balanced ascending and descending gaits of a two-legged robot, *International Journal of Humanoid Robotics* **4** (2007) 717–751.
29. P. R. Vundavilli and D. K. Pratihar, Dynamically balanced optimal gaits of a ditch-crossing biped robot, *Rob Auton Syst* **58** (2010) 349–361.
30. P. R. Vundavilli and D. K. Pratihar, Soft computing-based gait planners for a dynamically balanced biped robot negotiating sloping surfaces, *Appl Soft Comput* **9** (2009) 191–208.
31. X. Luo, D. Xia and C. Zhu, Impact dynamics-based torso control for dynamic walking biped robots, *International Journal of Humanoid Robotics* **15** (2018).
32. M. Raj, V. B. Semwal and G. C. Nandi, Multiobjective optimized bipedal locomotion, *International Journal of Machine Learning and Cybernetics* **10** (2019) 1997–2013.
33. V.-H. Dau, C.-M. Chew and A.-N. Poo, Achieving energy-efficient bipedal walking trajectory through GA-based optimization of key parameters, *International Journal of Humanoid Robotics* **6** (2009) 609–629.
34. C. Niehaus, T. Röfer and T. Laue, Gait optimization on a humanoid robot using particle swarm optimization, in *Proceedings of the Second Workshop on Humanoid Soccer Robots in Conjunction with The* (2007), pp. 1–7.
35. L. Gong, R. Zhao, J. Liang, L. Li, M. Zhu, Y. Xu, X. Tai, X. Qiu, H. He, F. Guo, J. Yao, Z. Chen and C. Zhang, Generation of walking motions for the biped ascending slopes based on genetic algorithm, in *Lecture Notes in Computer Science (Including Subseries Lecture Notes in Artificial Intelligence and Lecture Notes in Bioinformatics)* (Springer Verlag, 2018), pp. 201–209.
36. T. Hemker, M. Stelzer, O. von Stryk and H. Sakamoto, Efficient walking speed optimization of a humanoid robot, *Int J Rob Res* **28** (2009) 303–314.
37. K. Wolff, D. Sandberg and M. Wahde, Evolutionary optimization of a bipedal gait in a physical robot, in *2008 IEEE Congress on Evolutionary Computation, CEC 2008* (2008), pp. 440–445.
38. M. K. Muni, D. R. Parhi and P. B. Kumar, Improved motion planning of humanoid robots using bacterial foraging optimization, *Robotica* **39** (2021) 123–136.
39. L.-Y. Wang, Z. Liu, X.-J. Zeng and Y. Zhang, Gait control of humanoid robots via fuzzy logic and iterative optimization, in *Proceedings of the 30th Chinese Control Conference* (IEEE, 2011), pp. 3931–3936.
40. L. Roussel, C. Canudas-De-Wit and A. Goswami, Generation of energy optimal complete gait cycles for biped robots, in *Proceedings. 1998 IEEE International Conference on Robotics and Automation (Cat. No. 98CH36146)* (1998), pp. 2036–2041.
41. F. M. Silva and J. A. T. Machado, Energy analysis during biped walking, in *Proceedings 1999 IEEE International Conference on Robotics and Automation (Cat. No. 99CH36288C)* (1999), pp. 59–64.
42. P. H. Channon, S. H. Hopkins and D. T. Pham, A variational approach to the optimization of gait for a bipedal robot, *Proc Inst Mech Eng C J Mech Eng Sci* **210** (1996) 177–184.
43. Y. Uno, M. Kawato and R. Suzuki, Formation and control of optimal trajectory in human multijoint arm movement, *Biological Cybernetics* **1989 61:2** **61** (1989) 89–101.
44. SoftBank Robotics Developer Center, Kinematics Data: Links, Joints, and Body Frames, Available at: <https://developer.softbankrobotics.com/nao6/nao-documentation/nao-developer-guide/kinematics-data>. [Accessed: 15-Aug-2021].
45. SoftBank Robotics Developer Center, The masses and CoM positions for NAO, Available at: <https://developer.softbankrobotics.com/nao-naoqi-2-1/nao-documentation/nao-technical-guide/nao-h25/h25-masses>. [Accessed: 15-Aug-2021].
46. K. S. Fu, R. C. Gonzalez, and C. S. G. Lee, *Robotics: control, sensing, vision, and intelligence*, Vol. 1, Tata McGraw-Hill Education, New York, USA, 1987.

47. M. Vukobratović and J. Stepanenko, On the stability of anthropomorphic systems, *Math Biosci* **15** (1972) 1–37.
48. D. K. Pratihara, V. Pandu Ranga and R. Rajendra, Humanoid Body Control Using Neural Networks and Fuzzy Logic, in *Humanoid Robotics: A Reference* (2018), pp. 1–25.
49. Q. Li, A. Takanishi and I. Kato, A biped walking robot having a ZMP measurement system using universal force-moment sensors, in *Proceedings IROS'91: IEEE/RSJ International Workshop on Intelligent Robots and Systems '91* (1991), pp. 1568–1573.
50. P. Sardain and G. Bessonnet, Forces acting on a biped robot. Center of pressure-zero moment point, *IEEE Transactions on Systems, Man, and Cybernetics-Part A: Systems and Humans* **34** (2004) 630–637.
51. S. Kajita, H. Hirukawa, K. Harada and K. Yokoi, Introduction to Humanoid Robotics, in *Springer Tracts in Advanced Robotics* (Springer Berlin Heidelberg, Berlin, Heidelberg, 2014).
52. J. Nishii, K. Ogawa and R. Suzuki, The optimal gait pattern in hexapods based on energetic efficiency, in *Proc. 3rd International Symposium on Artificial Life and Robotics, Beppu* (1998), pp. 106–109.
53. J. Cristiano, D. Puig and M. A. Garcia, On the maximum walking speed of NAO humanoid robots, in *XII Workshop of Physical Agents* (2011), pp. 3–7.
54. J. Kennedy and R. Eberhart, Particle swarm optimization, *Proceedings of ICNN'95 - International Conference on Neural Networks* **4** (n.d.) 1942–1948.
55. Mostapha Kalami Heris, Particle Swarm Optimization in MATLAB, n.d. . Available at: URL: <https://yarpiz.com/50/ypea102-particle-swarm-optimization>. [Accessed: 15-Aug-2021].
56. K. Deb and R. B. Agrawal, Simulated binary crossover for continuous search space, *Complex Systems* **9** (1995) 115–148.
57. K. Deb, M. Goyal and others, A combined genetic adaptive search (GeneAS) for engineering design, *Computer Science and Informatics* **26** (1996) 30–45.
58. Z. Sun and N. Roos, An energy efficient dynamic gait for a Nao robot, in *2014 IEEE International Conference on Autonomous Robot Systems and Competitions (ICARSC)* (2014), pp. 267–272.
59. S. Omran, S. Sakka and Y. Aoustin, Effects of COM Vertical Oscillation on Joint Torques during 3D Walking of Humanoid Robots, *International Journal of Humanoid Robotics* **13** (2016), pp 1650019(1)-1650019(18).
60. R. K. Mandava and P. R. Vundavilli, Study on influence of hip trajectory on the balance of a biped robot, *Lecture Notes in Electrical Engineering* **394** (2017) 265–272.
61. Y. Fujimoto, Minimum energy biped running gait and development of energy regeneration leg, in *The 8th IEEE International Workshop on Advanced Motion Control, 2004. AMC '04.* (2004), pp. 415–420.
62. F. Farzadpour, M. Danesh and S. M. TorkLarki, Development of multi-phase dynamic equations for a seven-link biped robot with improved foot rotation in the double support phase, *Proc Inst Mech Eng C J Mech Eng Sci* **229** (2015) 3–17.



Pushpendra Gupta is pursuing his Ph.D. in the Department of Mechanical Engineering of the Indian Institute of Technology Kharagpur, India. He received his M. Tech (Gold Medallist) in the Production Engineering Department from the National Institute of Technology Agartala, India in 2015. He received his B. Tech in Mechanical and Automation Engineering from Maharshi Dayanand University Rohtak, India in 2011. He has also worked as a faculty member for two and a half years at MITRC Alwar, Rajasthan, India, prior joining to IIT Kharagpur. His current research as a PhD Research Scholar is focused on optimal gait generation in biped locomotion of humanoid robots. His research interests include humanoid robots, soft computing approaches, multi-, and many-objective optimization.



Dr. Dilip Kumar Pratihara received his Ph.D. from Indian Institute of Technology Kanpur, India, in 2000. He received University Gold Medal, A.M. Das Memorial Medal, Institution of Engineers' (I) Medal, INSA Teachers' Award 2020, New Code of Education 2021 Award, Distinguished Alumnus Award 2021 from National Institute of Technology, Durgapur, India, Technologist of the Year 2022 Award from IEEE India Council, Institute Chair Professor Award 2022 from, IIT Kharagpur, India, and others. He completed his post-doctoral studies in Japan,

and then, in Germany under the Alexander von Humboldt (AvH) Fellowship Programme. He is working now as a Professor of Indian Institute of Technology Kharagpur, India. His research areas include Robotics, Soft Computing, Manufacturing Science, and others. He has made significant contributions in his fields of research. He has authored/co-authored three textbooks, four reference books and edited one book. He has developed three on-line NPTEL courses, such as "Traditional

and Non-Traditional Optimization Tools”, “Robotics” and “Fuzzy Logic and Neural Networks”. He has guided 25 Ph.D.s. He has filed four patents, and been granted one Copyright. He has completed a number of sponsored projects. He is in editorial board of a few International Journals. He is an Associate Editor of two International Journals. He has been elected as a Fellow of Institution of Engineers (I), MASME and SMIEEE.



Kalyanmoy Deb is University Distinguished Professor and Koenig Endowed Chair Professor at Department of Electrical and Computer Engineering in Michigan State University, USA. He was an International Visiting Professor at Indian Institute of Technology Kharagpur during the course of this study. Prof. Deb's research interests are in evolutionary optimization and their application in multi-criterion optimization, modeling, and machine learning. He was awarded IEEE Evolutionary Computation Pioneer Award for his sustained work in EMO, Infosys Prize, TWAS Prize in Engineering Sciences, CajAstur Mamdani Prize, Distinguished Alumni Award from IIT Kharagpur, Edgeworth-Pareto award, Bhatnagar Prize in Engineering Sciences, and Bessel Research award from Germany. He is fellow of IEEE and ASME. He has published over 570 research papers with Google Scholar citation of over 189,000 with h-index 127. He is in the editorial board on 10 major international journals. More information about his research contribution can be found from <https://www.coin-lab.org>.